

# Oscillation Measurements with Upgraded Conventional Neutrino Beams

March 6, 2001

V. Barger,<sup>1</sup> R. Bernstein,<sup>4</sup> A. Bueno,<sup>2</sup> M. Campanelli,<sup>2</sup> D. Casper,<sup>3</sup>  
F. DeJongh,<sup>4</sup> S. Geer,<sup>4</sup> M. Goodman,<sup>5</sup> D.A. Harris,<sup>4</sup> K.S. McFarland,<sup>6</sup>  
N. Mokhov,<sup>4</sup> J. Morfin,<sup>4</sup> J. Nelson,<sup>7</sup> F. Pietropaolo,<sup>8</sup> R. Raja,<sup>4</sup> J. Rico,<sup>2</sup>  
A. Rubbia,<sup>2</sup> H. Schellman,<sup>9</sup> R. Shrock,<sup>10</sup> P. Spentzouris,<sup>4</sup> R. Stefanski,<sup>4</sup>  
L. Wai,<sup>11</sup> K. Whisnant<sup>12</sup>

<sup>1</sup> *University of Wisconsin, Madison, WI 53706*

<sup>2</sup> *Institut für Teilchenphysik, ETHZ, CH-8093, Zürich, Switzerland*

<sup>3</sup> *University of California Irvine, Irvine, CA 92697*

<sup>4</sup> *Fermi National Accelerator Laboratory, Batavia, IL 60510*

<sup>5</sup> *Argonne National Laboratory, Argonne, IL 60439*

<sup>6</sup> *University of Rochester, Rochester, NY 14627*

<sup>7</sup> *University of Minnesota, Minneapolis, MN 55455*

<sup>8</sup> *University of Padova, Padova, Italy*

<sup>9</sup> *Northwestern University, Evanston, IL 60208*

<sup>10</sup> *State University of New York Stony Brook, Stony Brook, NY 11794*

<sup>11</sup> *Stanford University, Stanford, CA*

<sup>12</sup> *Iowa State University, Ames, IA 50011*

## Abstract

We consider the  $\nu_\mu \rightarrow \nu_e$  oscillation measurements that would be possible at upgraded 1 GeV and multi-GeV conventional neutrino sources driven by future megawatt-scale proton drivers. If these neutrino superbeams are used together with detectors that are an order of magnitude larger than those presently foreseen, we find that the sensitivity to  $\nu_\mu \rightarrow \nu_e$  oscillations can be improved by an order of magnitude beyond the next generation of accelerator based experiments. In addition, over a limited region of parameter space, the neutrino mass hierarchy can be determined with a multi-GeV long baseline beam. If the Large Mixing Angle MSW solution correctly describes the solar neutrino deficit, there is a small corner of allowed parameter space in which maximal CP-violation in the lepton sector might be observable at a 1 GeV medium baseline experiment. Superbeams with massive detectors would therefore provide a useful tool en route to a neutrino factory, which would permit a further order of magnitude improvement in sensitivity, together with a more comprehensive check of CP-violation and the oscillation framework.

# 1 Prologue

We have recently completed a six-month study of the prospective physics program at a neutrino factory, evaluated as a function of the stored muon energy (up to 50 GeV) and the number of useful muon decays per year (in the range from  $10^{19}$  to  $10^{21}$ ). The basic conclusions presented in our report [1] were that: (1) There is a compelling physics case for a neutrino factory [2] with a muon beam energy of about 20 GeV or greater, and (2) The neutrino factory should provide at least  $O(10^{19})$  useful decays per year initially, and ultimately at least  $O(10^{20})$  decays per year. The oscillation physics that can be pursued using initial electron-neutrino ( $\nu_e$ ) and electron-antineutrino ( $\bar{\nu}_e$ ) beams provides the primary motivation for a neutrino factory. In particular we found that with  $2 \times 10^{20}$  decays per year, after a few years of running:

- (i) A  $\nu_e \rightarrow \nu_\mu$  oscillation signal could be observed, and the associated amplitude parameter  $\sin^2 2\theta_{13}$  measured, for oscillation amplitudes approaching  $10^{-4}$ , three orders of magnitude below the currently excluded region and two orders of magnitude below the region expected to be probed by the next generation of long-baseline accelerator based experiments.
- (ii) Once a  $\nu_e \rightarrow \nu_\mu$  signal has been established in a long baseline experiment, matter effects can be exploited to determine the sign of the difference between the squares of the neutrino mass eigenstates  $\delta m_{32}^2$ , and hence determine the neutrino mass hierarchy.
- (iii) If the large mixing angle MSW solution describes the solar neutrino deficit, and if  $\sin^2 2\theta_{13}$  is not less than one to two orders of magnitude below the currently excluded region, a comparison of  $\nu_e \rightarrow \nu_\mu$  and  $\bar{\nu}_e \rightarrow \bar{\nu}_\mu$  oscillation probabilities would enable the measurement of (or stringent limits on) CP-violation in the lepton sector.
- (iv) Measurements of, or stringent limits on, all of the observable  $\nu_e \rightarrow \nu_X$  oscillation modes together with the observable  $\nu_\mu \rightarrow \nu_X$  modes, would enable a comprehensive test of the assumed oscillation framework.

In parallel with our neutrino factory physics study, a companion design study [3] was conducted to determine the feasibility of constructing a neutrino factory, and to identify the associated R&D issues. The design study concluded that a neutrino factory with the desired parameters was indeed feasible, although it would require a vigorous and well supported R&D program. Recognizing that the R&D would take some time, and that a neutrino factory would require a very intense (megawatt-scale) proton driver, it is reasonable to consider the neutrino oscillation physics program that could be conducted using a MW-scale proton driver en route to a neutrino factory. In our neutrino factory physics study report we recommended that an additional study of the oscillation physics potential at these “neutrino superbeams” be undertaken.

The present document, which can be considered as an addendum to our initial report, presents results from a study of oscillation physics at 1 GeV and multi-GeV neutrino superbeams.

## 2 Introduction

In this report we consider the oscillation physics capabilities of neutrino “superbeams”, which we define as conventional neutrino beams produced using megawatt-scale high-energy proton drivers. Examples of appropriate proton drivers are (i) the proposed 0.77 MW 50 GeV proton synchrotron at the Japan Hadron Facility (JHF) [4], (ii) a 4 MW upgraded version of the JHF, (iii) a new  $\sim 1$  MW 16 GeV proton driver that would replace the existing 8 GeV Booster at Fermilab, or (iv) a fourfold intensity upgrade of the 120 GeV Fermilab Main Injector (MI) beam (to 1.6 MW) that would become possible once the upgraded (16 GeV) Booster was operational. The 4 MW 50 GeV JHF and the 16 GeV upgraded Fermilab Booster, are both suitable proton drivers for a neutrino factory. Hence a neutrino superbeam might provide a neutrino physics program en route to a neutrino factory.

The next generation of accelerator based long-baseline neutrino oscillation experiments are expected to confirm the  $\nu_\mu \rightarrow \nu_\tau$  oscillation interpretation of the atmospheric muon-neutrino deficit, and begin to measure the associated oscillation parameters with modest statistical precision. To make a significant improvement in oscillation measurements beyond the next generation of experiments will require a significant increase in signal statistics. A factor of a few increased neutrino beam flux will not be sufficient unless there is also a substantial increase in detector mass. We will therefore assume that superbeam experiments will use detectors an order of magnitude larger than those currently under construction. Hence, a superbeam experiment would yield data samples with a statistical sensitivity a factor of at least  $\sqrt{40}$  better than expected for K2K [5], MINOS [6], OPERA [7], and ICARUS [8]. Clearly, this would enable significant progress in pinning down  $\nu_\mu \rightarrow \nu_\tau$  oscillations, for example. However, the neutrino oscillation physics program at a superbeam would have to justify the substantial investment associated with the detector. For example, a detector costing ten times the MINOS detector would be of order \$300M. Hence, more precise measurements of the quantities already measured by the next generation experiments may be insufficient motivation for a superbeam.

The primary motivation for a neutrino superbeam is likely to be the search for, and measurement of,  $\nu_\mu \rightarrow \nu_e$  oscillations. The observation of this mode would enable the associated amplitude parameter  $\sin^2 2\theta_{13}$  to be determined, and open the way for the determination of the sign of the differences between the squares of the neutrino mass eigenstates  $\delta m_{32}^2$ , and hence the determination of the neutrino mass hierarchy. A comparison between the oscillation probabilities for  $\nu_\mu \rightarrow \nu_e$  and  $\bar{\nu}_\mu \rightarrow \bar{\nu}_e$  oscillations might also be sensitive to CP-violation in the lepton sector. Hence, in principle the  $\nu_\mu \rightarrow \nu_e$  mode at a superbeam can offer a handle on much of the physics that the  $\nu_e \rightarrow \nu_\mu$  mode offers at a neutrino factory. Indeed, for low energy neutrino beams ( $E_\nu < 10$  GeV) the neutrino fluxes at a superbeam are comparable or larger than the corresponding neutrino factory fluxes (see Table 1). However, there is a substantial qualitative difference between searching for  $\nu_e$  appearance at a superbeam and  $\nu_\mu$  appearance at a neutrino factory. The signal signature at a superbeam is the appearance of an isolated electron (or positron) in a charged current (CC) event. As we will see, this signature is plagued with backgrounds at the level of  $O(1\%)$  of the total CC rate. For comparison, the signal signature at a neutrino factory is the appearance in a CC event of a wrong-sign muon (a muon of the opposite charge-sign to that of the muons stored in the muon ring). This signature enables backgrounds to be suppressed to the

Table 1: Neutrino event rates assuming no oscillations, compared with intrinsic beam backgrounds for conventional and muon-derived beams of comparable energies. The calculations assume a 1.6 MW proton source is used for the MINOS-type beam, the neutrino factories provide  $2 \times 10^{20}$  muon decays per year in the beam-forming straight section, and the detector is 732 km downstream of the neutrino source.

Beam (Signal: $\nu_\mu \rightarrow \nu_e$ )	$\langle E_\nu \rangle$ (GeV)	$\nu_\mu$ CC Events (per kton-year)	$\nu_e/\nu_\mu$ Fraction
MINOS-LE	3.5	1800	0.012
MINOS-ME	7	5760	0.009
MINOS-HE	15	12800	0.006

Beam (Signal: $\nu_e \rightarrow \nu_\mu$ )	$\langle E_\nu \rangle$ (GeV)	$\nu_e$ CC Events (per kton-year)	$\nu_\mu/\nu_e$ Fraction
4.5 GeV $\mu$ Ring	3.5	400	0
9.1 GeV $\mu$ Ring	7	3700	0
18.2 GeV $\mu$ Ring	15	31400	0
30 GeV $\mu$ Ring	20	72600	0

level of  $O(0.01\%)$  of the total CC rate [1]. Hence, to understand the oscillation physics potential at a superbeam we must have a good understanding of the backgrounds and the systematic uncertainties associated with the background subtraction.

In Section 3 of this report we begin by discussing the properties of conventional neutrino beams. The motivation for large mass detectors with excellent background rejection is discussed in Section 4. The most important backgrounds to  $\nu_\mu \rightarrow \nu_e$  and  $\bar{\nu}_\mu \rightarrow \bar{\nu}_e$  oscillations are discussed in Section 5. The physics capabilities of multi-GeV long baseline experiments and 1 GeV medium baseline experiments are discussed respectively in Sections 6 and 7. A summary is given in Section 8. Throughout we will use the three-flavor oscillation framework which is reviewed in Appendix 1, with the “leading” oscillation parameters  $\sin^2 2\theta_{23}$  and  $\delta m_{32}^2$  determined by the atmospheric neutrino deficit, and the sub-leading parameters  $\sin^2 2\theta_{12}$  and  $\delta m_{21}^2$  determined by the solar neutrino deficit. This choice is appropriate if the LSND effect [9] is not confirmed (by MiniBooNE [10], for example). Should the LSND effect be confirmed, there is likely to be a strong physics case for a low intensity neutrino factory, which might be constructed on a relatively fast timescale with only a short R&D phase. The case for a separate superbeam program is less obvious (or at least different) in this case.

### 3 Beam characteristics and event rates

A conventional neutrino beam is produced using a primary proton beam to create a secondary beam of charged pions and kaons, which are then allowed to decay to produce a tertiary neutrino beam. The secondary beam can be charge-sign selected to produce either a neutrino beam from positive meson decays or an antineutrino beam from negative meson decays. The secondary particles, which are confined radially us-

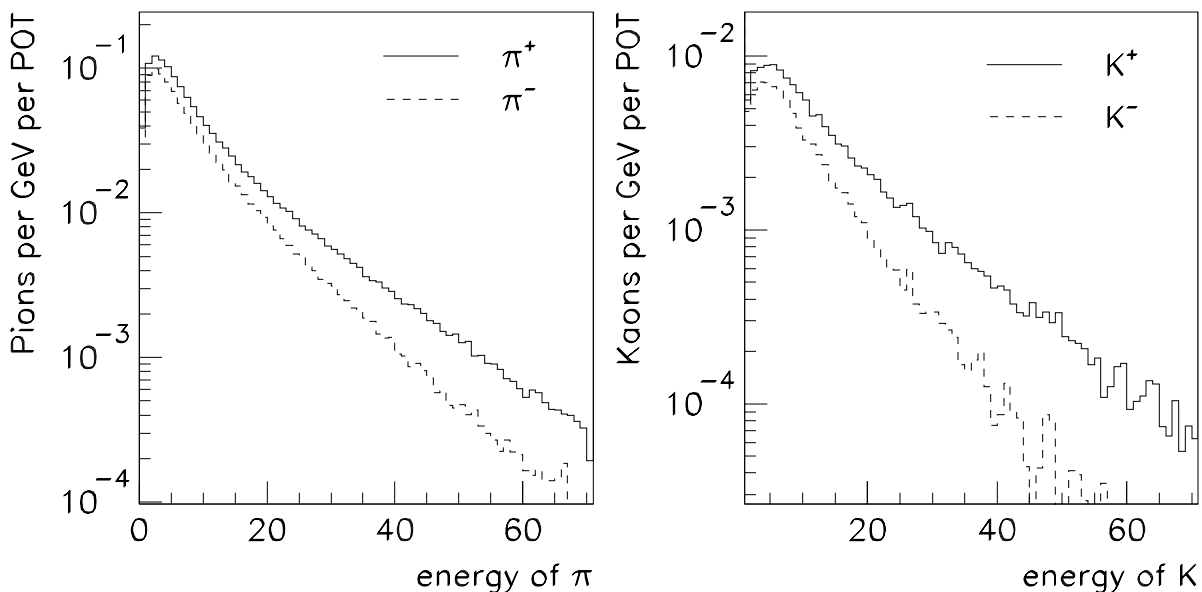


Figure 1: Differential spectra for pions (left) and kaons (right) produced when 120 GeV protons are incident on the MINOS target. The distributions are normalized to correspond to the number of particles per incident proton.

ing either a quadrupole channel or horn focusing, are allowed to decay in a long decay channel. The resulting neutrino beam consists mostly of muon neutrinos (or antineutrinos) from  $\pi^\pm \rightarrow \mu\nu_\mu$  decays, with a small “contamination” of electron neutrinos, electron antineutrinos, and muon antineutrinos from muon, kaon, and charmed meson decays. The fractions of  $\nu_e$ ,  $\bar{\nu}_e$  and  $\bar{\nu}_\mu$  in the beam depend critically on the beamline design.

Figure 1 shows the momentum spectrum of charged pions and kaons produced when a 120 GeV beam of protons strikes a 2 interaction length graphite target [11]. Note that at low momenta, positive and negative secondaries are created at comparable rates, but at higher momentum there is a marked asymmetry. For example, at 20 GeV the ratio of positive to negative secondaries is 3/2. Hence, for high energy beams there is a flux penalty in producing an antineutrino beam rather than a neutrino beam. This flux penalty increases with increasing beam energy.

For the two-body decays  $\pi \rightarrow \mu\nu_\mu$  and  $K \rightarrow \mu\nu_\mu$  there is a one to one correspondence between the energy of the parent meson and the energy of the neutrino at the far detector. For a parent particle of mass  $m_h$  and energy  $E_h$ , traveling in a direction  $\theta_{\nu h}$  with respect to the far detector, the neutrino energy is given by:

$$E_\nu = \frac{m_h^2 - m_\mu^2}{2m_h} \times \frac{m_h}{E_h - p_h \cos \theta_{\nu h}} \approx E_h \frac{m_h^2 - m_\mu^2}{m_h^2} \frac{1}{1 + \gamma^2 \theta_{\nu h}^2}. \quad (1)$$

For a perfectly focused beam  $\theta_{\nu h} = 0$ , and  $E_\nu = 0.42E_h$  for pion decays and  $0.95E_h$  for kaon decays. In practice the beamline is designed to focus pions within a given momentum window. A broader pion momentum acceptance will result in a higher flux of neutrinos in the forward direction, but will also result in a broader energy spread within the neutrino beam. The flux of neutrinos per meson at the far detector is given

by:

$$\phi = BR \frac{1}{4\pi L^2} \left( \frac{m_h}{E_h - p_h \cos \theta_{\nu h}} \right)^2 \approx BR \frac{1}{4\pi L^2} \left( \frac{2\gamma}{1 + \gamma^2 \theta_{\nu h}^2} \right)^2, \quad (2)$$

where  $BR$  is the branching fraction for the appropriate meson decay,  $\gamma$  is the Lorentz boost of the decaying particle, and  $L$  is the distance to the detector. Note that the flux at the far detector has the familiar  $\gamma^2$  dependence, and since the cross-section increases linearly with  $\gamma$ , the event rate has a  $\gamma^3$  dependence. Figure 2 shows, for a perfectly focussed beam, the calculated  $\nu_\mu$  and  $\bar{\nu}_\mu$  event rates per kton-year for the MINOS detector at  $L = 732$  km, assuming a total decay region of 725 m. Note that for a realistic focusing system the neutrino flux would be reduced, typically by a factor of 2 or 3. The calculation shown in Fig. 2 is for  $15 \times 10^{20}$  120 GeV protons striking a graphite target (4 x NuMI [12] for 1 year) similar to the one being constructed for the MINOS beam [11], with the beamline set to focus either positive or negative pions. Also shown are the corresponding event rates at a neutrino factory in which there are  $2 \times 10^{20}$  useful muon decays, with  $E_\mu = 10$  and 20 GeV.

The total CC event rates for 1.6 MW NuMI low, medium, and high energy superbeams are compared in Table 1 with the corresponding (same  $\langle E_\nu \rangle$ ) rates at a neutrino factory. Note that the rates at a neutrino factory rapidly exceed the corresponding conventional beam rates for neutrino beam energies exceeding about 10 GeV. For lower energies, conventional beams provide higher rates although the beam is not background free, and the electron appearance signal is experimentally challenging.

Finally, the decay channel for a very long-baseline superbeam must fit within the viable rock layer below the proton driver. At Fermilab this rock layer is  $\sim 200$  m deep, below which there is a deep aquifer. This limits the length of the decay pipe to less than  $200\text{m} \times \sin \theta$ , where the dip angle  $\theta$  depends on the baseline:  $L = 12756 \times \sin \theta$  km. In fact the length of the decay region is further restricted by the depth of rock used to bury the proton driver, bend the proton beam to the required direction, accommodate the target and focusing systems, and if there is a near detector, accommodate the associated shielding and near detector hall. Figure 3 shows the relative flux loss for different energy beamlines as a function of baseline length [13]. The calculation allows 30 m for the near detector shielding plus hall. For a baseline of 732 km,  $\theta = 3.3^\circ$  and the NuMI beam pipe length of 675 m is not restricted by the depth of the good rock. However for a far site at 7300 km (Fermilab  $\rightarrow$  Gran Sasso),  $\theta = 35^\circ$ , and the length of the decay channel is severely restricted, so that for the LE (ME) [HE] NuMI beams only 50% (25%) [13%] of the pions would decay in the channel. Clearly, decay channel length restrictions must be taken into account in calculating the fluxes for very long baselines ( $> 3000$  km). For trans-Atlantic or trans-Pacific baselines there is a premium on minimizing the shielding and detector hall length for the near detector, minimizing the length of the targeting hall, using high-field dipoles to rapidly bend the 120 GeV proton beam to the required direction, and perhaps considering a “roller-coaster” geometry for the proton beam.

## 4 Large detectors and low backgrounds

Our first physics goal is the observation of  $\nu_\mu \rightarrow \nu_e$  oscillations. Since, to a good approximation the oscillation probability is proportional to the amplitude parameter

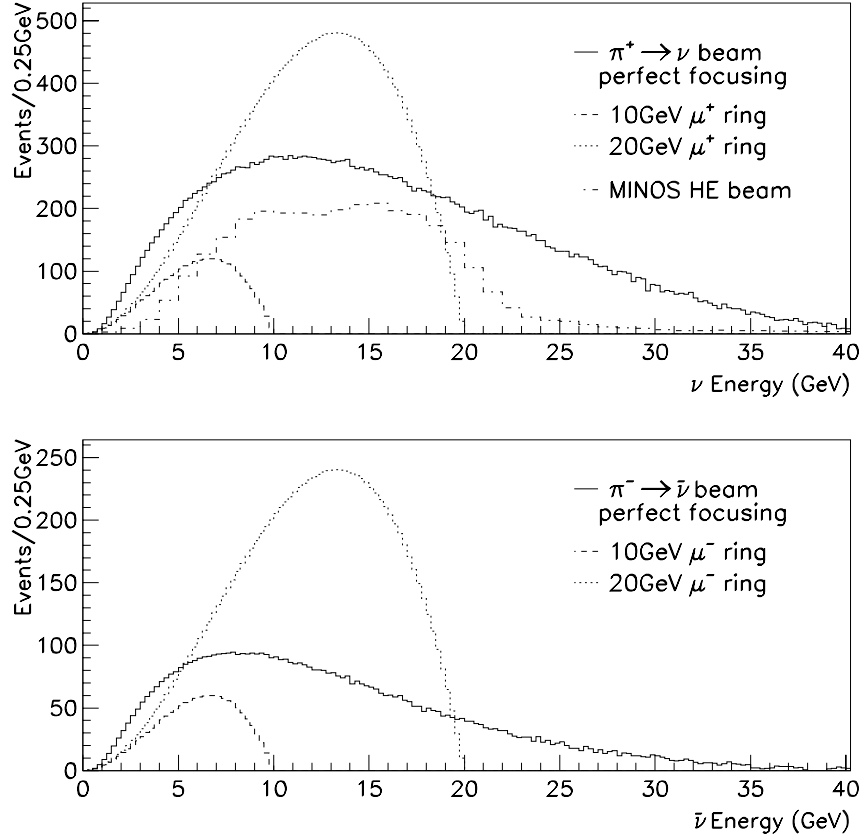


Figure 2: Differential  $\nu_\mu$  (top) and  $\bar{\nu}_\mu$  (bottom) event rates in the MINOS detector 732 km downstream of a perfectly focused beam of pions and kaons produced when  $15 \times 10^{20}$  120 GeV protons are incident on a graphite target ( $4 \times$  NuMI for 1 year). The top panel also shows the predicted spectrum for a realistic focussing system, namely the MINOS HE beam (as indicated). Note that the rates are expected to be a factor of 2 or 3 less for a realistic system than for a perfectly focussed beam. The distributions are compared to the corresponding  $\nu_e$  event rates 732 km downstream of 10 GeV and 20 GeV muon storage rings driven by a 1.6 MW 16 GeV proton source.

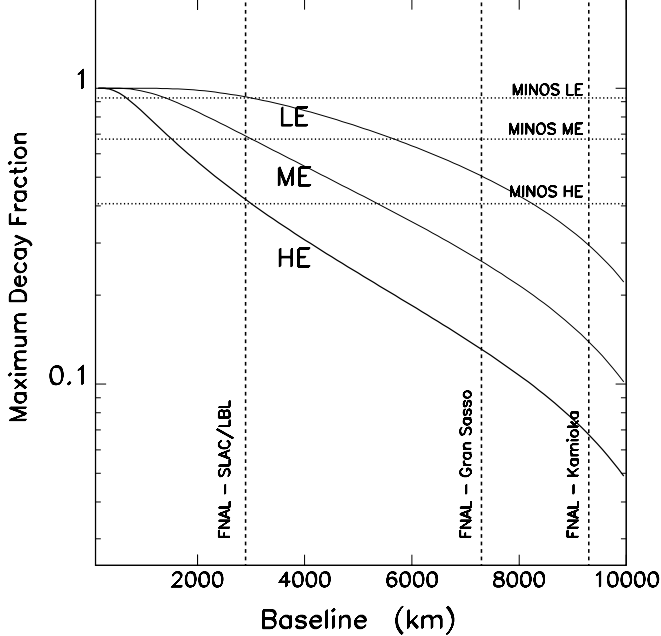


Figure 3: Fraction of  $\pi^\pm$  that decay in a channel of maximum length within a 200 m deep rock layer, shown as a function of baseline for three different average NuMI beam energies: 3.5 GeV (LE), 7 GeV (ME), and 15 GeV (HE). For convenience, distances from Fermilab to SLAC/LBNL, Gran Sasso, and Kamioka are indicated by vertical broken lines, and the decay fractions for the foreseen NuMI beams ( $L = 730$  km) are indicated by dotted horizontal lines.

$\sin^2 2\theta_{13}$ , it is useful to define the  $\sin^2 2\theta_{13}$ -reach for a given experiment, which we define as that value of  $\sin^2 2\theta_{13}$  which would result in a signal that is 3 standard deviations above the background. Taking the atmospheric neutrino deficit oscillation scale  $\delta m_{32}^2$  to be in the center of the region indicated by the SuperKamiokande (SuperK) data, for a given proton driver, superbeam design, and baseline, we can calculate the  $\sin^2 2\theta_{13}$  reach once we specify (a) the data sample size  $D$  (kt-years), defined as the product of the detector fiducial mass, the efficiency of the signal selection requirements, and the number of years of data taking, (b) the background fraction  $f_B$ , defined as the background rate divided by the total CC rate for events that pass the signal selection requirements, and (c) the fractional uncertainty  $\sigma_{f_B}/f_B$ . Note that  $D$  determines the statistical uncertainty on the signal. For a fixed  $D$ ,  $f_B$  determines the statistical uncertainty on the background, and  $f_B \times \sigma_{f_B}/f_B$  determines the systematic uncertainty on the background subtraction.

Contours of constant  $\sin^2 2\theta_{13}$  reach that correspond to various values of  $\sigma_{f_B}/f_B$  are shown in the  $(f_B, D)$ -plane in Fig. 4 for  $E_\nu = 1$  GeV superbeams produced using 0.77 MW and 4 MW JHF proton drivers. The corresponding contours are shown in Fig. 5 for long-baseline 1.6 MW medium energy and high energy NuMI superbeams. The contours have a characteristic shape. At sufficiently large  $D$  the  $\sin^2 2\theta_{13}$  sensitivity is limited by the systematic uncertainty on the background subtraction, and the reach does not significantly improve with increasing dataset size. The contours are therefore vertical in this region of the figures. At sufficiently small  $D$  the sensitivity of the  $\nu_\mu \rightarrow \nu_e$  appearance search is limited by signal statistics, and further reductions in  $f_B$  do not improve the  $\sin^2 2\theta_{13}$  reach. The contours are therefore horizontal in this

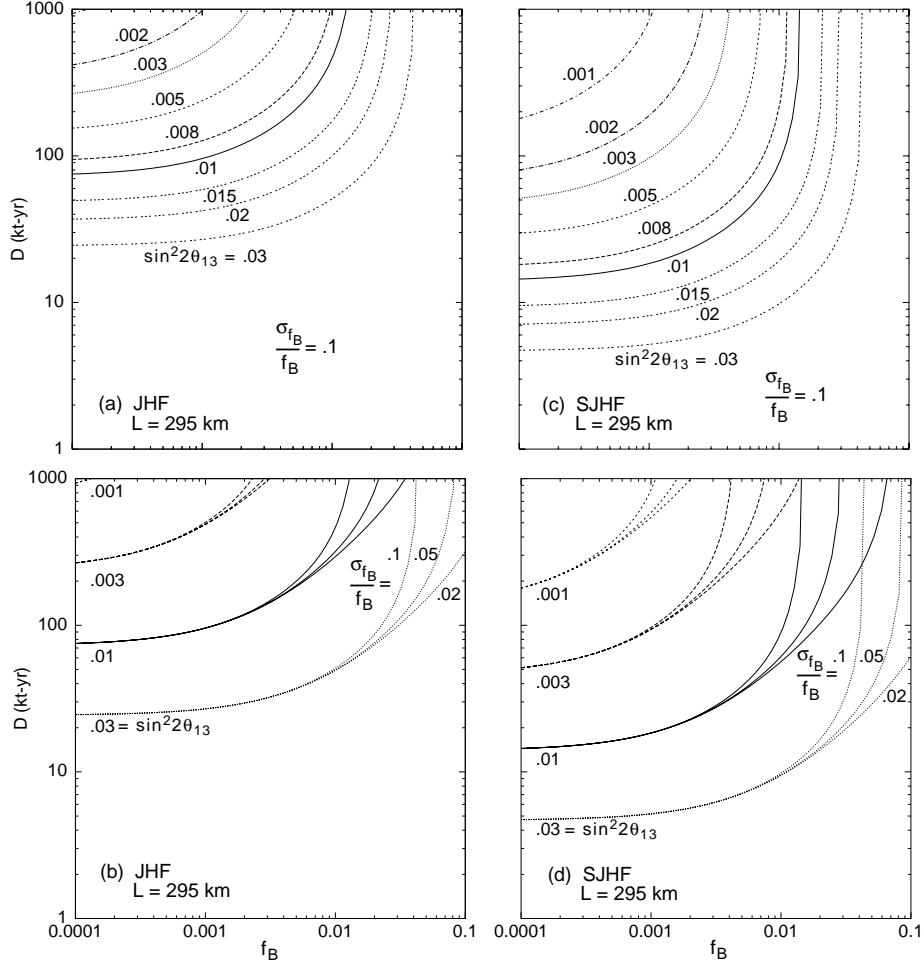


Figure 4: Contours of constant  $\sin^2 2\theta_{13}$  reach that correspond to a  $\nu_e \rightarrow \nu_\mu$  signal that is 3 standard deviations above the background [13]. The contours are shown in the  $(D, f_B)$ -plane, where  $D$  is the data-sample size and  $f_B$  the background rate divided by the total CC rate. The contours are shown for the 0.77 MW (left-hand plots) and 4.0 MW (right-hand plots) JHF scenarios with  $L = 295$  km. The top panels show curves for  $\sigma_{f_B}/f_B = 0.1$ , while the bottom panels show curves for  $\sigma_{f_B}/f_B = 0.1, 0.05$ , and  $0.02$ .

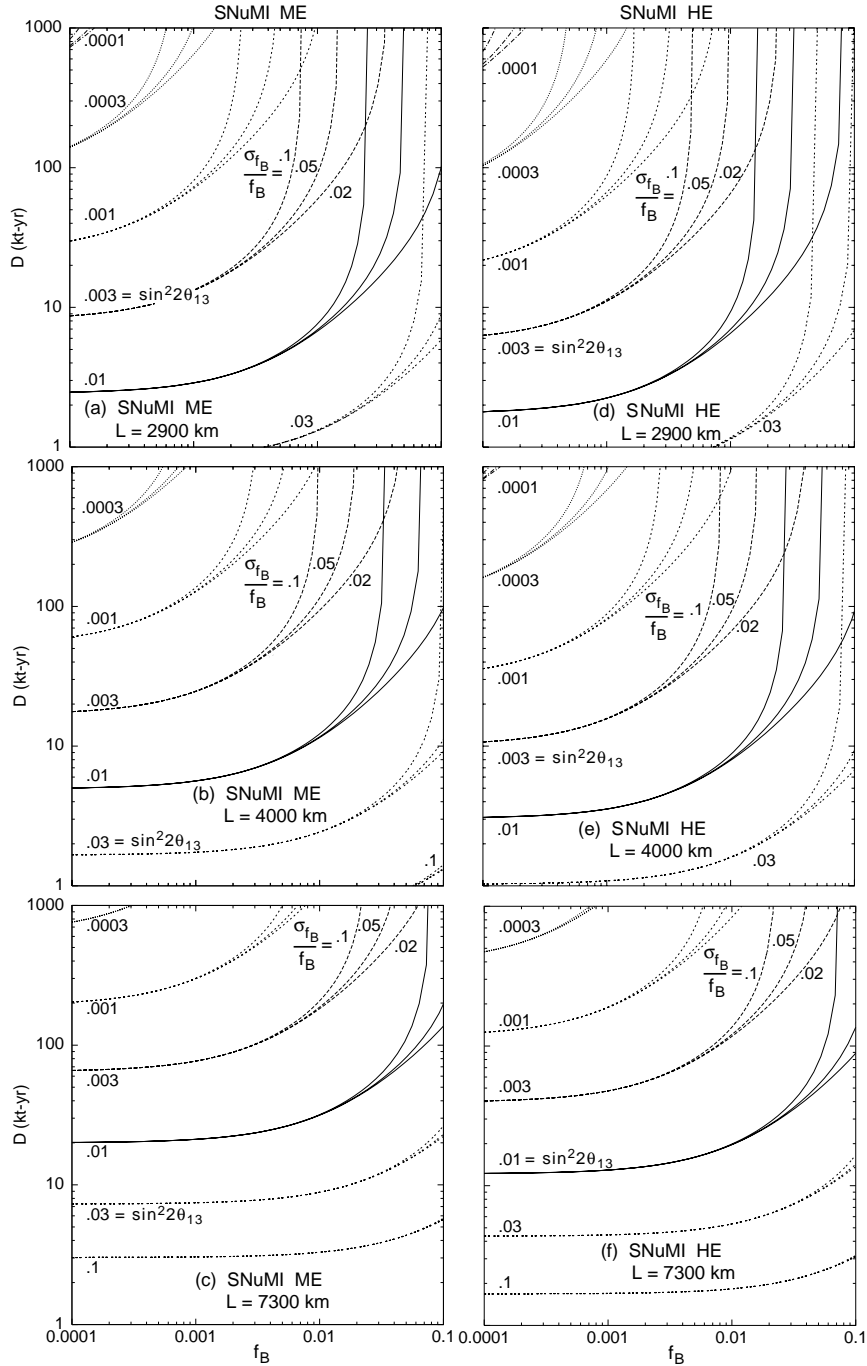


Figure 5: Contours of constant  $\sin^2 2\theta_{13}$  reach [13] that correspond to a  $\nu_e \rightarrow \nu_\mu$  signal that is 3 standard deviations above the background, at upgraded 1.6 MW NuMI ME (left) and HE (right) beams. The contours are shown in the  $(D, f_B)$ -plane, where  $D$  is the data-sample size and  $f_B$  the background rate divided by the total CC rate. The contours are shown for  $L = 2900$  (top), 4000 (center), and 7300 km (bottom). Curves are shown for systematic uncertainties on the background subtraction  $\sigma_{f_B}/f_B = 0.1, 0.05, \text{ and } 0.02$ .

region of the  $(f_B, D)$ -plane. Note that the next generation of neutrino experiments are expected to achieve  $\sin^2 2\theta_{13}$  reaches of  $\sim 0.03$ . Now consider as examples the 4 MW JHF beam, and the 1.6 MW NuMI beam with  $L = 2900$  km. Taking  $\sigma_{f_B}/f_B = 0.05$ , an inspection of the figures leads us to conclude that if we wish to improve the  $\sin^2 2\theta_{13}$  sensitivity an order of magnitude beyond the next generation of experiments, in the limit of very massive detectors at the JHF (NuMI) superbeams, we can only tolerate background fractions  $f_B < 0.007$  (0.004). Achieving the required background rejection in a water cerenkov detector seems challenging. Achieving the required detector masses with detector technologies that can meet the  $f_B$  requirements also seems challenging. Hence an understanding of the physics capabilities at a superbeam necessarily begins with an understanding of the parameters  $D$ ,  $f_B$ , and  $\sigma_{f_B}/f_B$  that can be achieved with realistic (but futuristic) detectors.

In the following section we consider the backgrounds, and for realistic futuristic detectors,  $D$  and  $f_B$ . This will enable us to use the  $(f_B, D)$  figures to determine the  $\sin^2 2\theta_{13}$  sensitivity at various superbeams.

## 5 Backgrounds to $\nu_\mu \rightarrow \nu_e$ oscillations

Backgrounds play a critical role in determining the sensitivity of a superbeam experiment to  $\nu_\mu \rightarrow \nu_e$  oscillations. In our neutrino factory studies [1] it was straightforward to obtain backgrounds to the  $\nu_e \rightarrow \nu_\mu$  search at the  $f_B \sim 10^{-4}$  level by cutting on the final state muon momentum. However, for conventional neutrino beams reducing the background rates below  $10^{-2}$  of the total CC rate is not trivial and would require significant reductions in the beam flux and signal selection efficiency. There are four important sources of background in a  $\nu_e$  appearance search at a superbeam: (i) electron-neutrinos produced in the initial beam, (ii) neutral current (NC) neutrino interactions in which a  $\pi^0$  is mis-identified as an electron, (iii) CC  $\nu_\mu$  interactions in which a  $\pi^0$  is mis-identified as an electron, and the muon is not identified, and (iv) events from  $\nu_\mu \rightarrow \nu_\tau$  oscillations followed by  $\nu_\tau$  CC interactions and either  $\tau \rightarrow e + X$  decays, or  $\tau \rightarrow \pi^0 + X$  decays in which the  $\pi^0$  fakes an electron. In the following we discuss these backgrounds and how, for different detector technologies, the backgrounds might be suppressed.

### 5.1 Electron-neutrino contamination

In a conventional neutrino beamline, muon neutrinos are produced in two-body pion- and kaon-decays. However, the charged and neutral kaons can also undergo 3-body decays to produce an electron neutrino (or antineutrino). Furthermore, secondary muons in the beamline can also decay to produce electron neutrinos. Generally speaking, higher primary proton beam energies yield higher kaon/pion ratios, and longer decay channels permit more muon decays. The expected electron neutrino background fractions are listed in Table 2 for the next generation of conventional neutrino beams. Note that for most of the beamlines listed the  $\nu_e$  background fraction is around the 1% level. The exceptions are the MiniBooNE beam (which benefits from a relatively low primary proton energy), and ORLaND [14] (which uses stopped muons). Since the electron neutrinos within the beam are created in three-body decays, the  $\nu_e$  energy spectrum is typically much broader than the  $\nu_\mu$  spectrum. This effectively means that

Table 2: Electron neutrino fractions and the fractional energy spreads for a selection of current (or next) generation conventional neutrino beams. Note that most beamlines produce a beam with a fractional energy spread between 30% and 50%, and a  $\nu_e$  contamination that ranges from 0.2% to 1.2%, for beams at or above 1 GeV.

Beamline	Proton Energy (GeV)	Peak $\nu_\mu$ Energy (GeV)	$\nu_e/\nu_\mu$ ratio	$\sigma_{E_\nu}/E_\nu$
K2K	12	1.4	0.7%	1.0
MINOS LE	120	3.5	1.2%	0.28
MINOS ME	120	7	0.9%	0.43
MINOS HE	120	15	0.6%	0.47
CNGS	400	18	0.8%	0.33
JHF wide	50	1	0.7%	1.0
JHF HE	50	5	0.9%	0.40
MiniBooNE	8	0.5	0.2%	0.50
ORLaND	1.3	0.0528	0.05%	0.38

there is always some fraction of the electron neutrino flux which overlaps in energy with the muon neutrino flux.

The  $\nu_e$  flux contributions from  $K^\pm$  and  $\mu^\pm$  decays can be reduced by decreasing the secondary particle momentum acceptance. The contributions from  $K_L$  decays can be reduced by putting large bends in the beamline immediately after the proton target. The neutral meson backgrounds are particularly dangerous for  $\bar{\nu}$  running because they give electron neutrinos in a  $\bar{\nu}_e$  appearance search, and the cross section for the  $\nu_e$  background is therefore twice as large as for the  $\bar{\nu}_e$  signal. It has been suggested [15] that a neutrino beam could be made with an extremely small  $\nu_e$  contamination by only accepting pions and kaons within a narrow momentum interval, and then rejecting neutrino events that have a total energy inconsistent with the expected neutrino beam energy. To understand how this might work we consider the correspondence between the neutrino beam energy spread and the contribution to  $f_B$  from the initial  $\nu_e$  flux, which comes from  $K^\pm$ ,  $\mu^\pm$ , and  $K_L$  decays. The ratio of the initial  $\nu_e$  flux to  $\nu_\mu$  flux is shown as a function of the fractional beam energy spread in Fig. 6 for a perfectly focussed secondary beam produced with 120 GeV primary protons on a 2 interaction length graphite target, followed by a 725 m long decay channel [11]. To achieve a background fraction that is no larger than 0.1% in either  $\nu$  or  $\bar{\nu}$  running would require a beamline with a momentum acceptance no larger than 10%. In addition, we must suppress the remaining  $\nu_e$  contribution from  $K_L$  decays (using one or more dipoles after the proton target) by factors in excess of 2.5 and 5 for  $\nu$  and  $\bar{\nu}$  running respectively. Noting that the effective  $\nu_\mu$  flux also decreases roughly linearly with the momentum acceptance, we conclude that, even for an idealized perfectly focussed beam, reducing the initial  $\nu_e$  contamination in the beam to 0.1% will result in an order of magnitude reduction in  $D$ .

An alternative way of decreasing the  $\nu_e$  contamination from kaon decays is to decrease the primary proton energy (from 120 GeV to something less). However, the

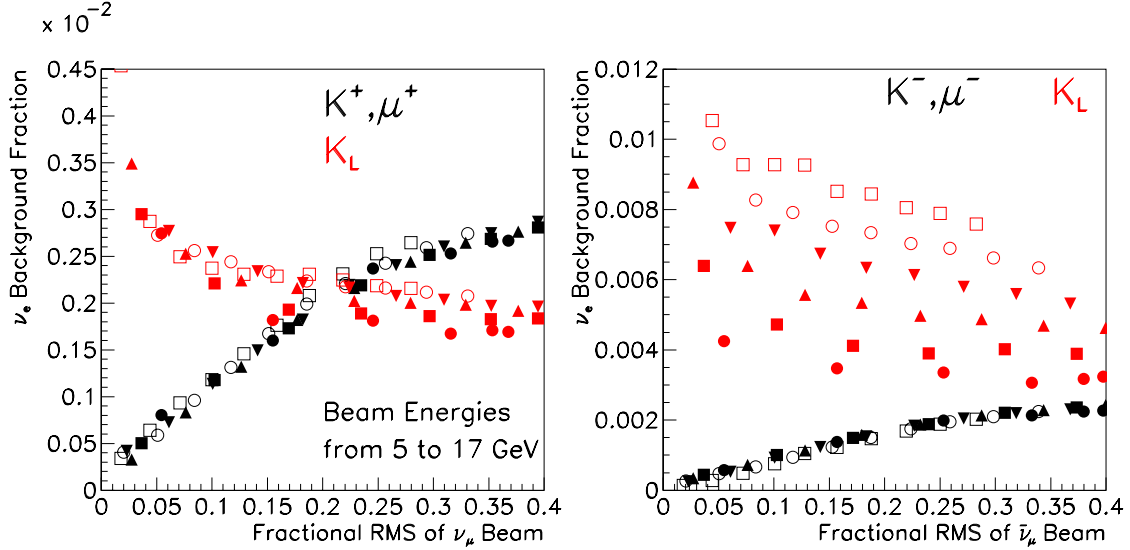


Figure 6: Fraction of  $\nu_e + \bar{\nu}_e$  events in a  $\nu_\mu$  (left) or  $\bar{\nu}_\mu$  (right) beam shown as a function of the fractional beam momentum spread. The various symbols correspond to different mean beam energies, from 5 GeV (filled circles) to 17 GeV (open squares). The distributions that increase (decrease) from left to right are the contributions from  $K^\pm, \mu^\pm$  ( $K_L$ ) decays.

MiniBooNE beam, which uses 8 GeV primary protons, is expected to achieve a  $\nu_e$  contamination of no better than 0.2%. Furthermore, even if kaon contributions are completely eliminated, muon decays still provide electron neutrinos.

In summary, for a multi-GeV neutrino beam, we would not expect a reduction in the momentum acceptance of the decay channel to significantly reduce the  $\nu_e$  contamination in the beam unless we are willing to accept a large reduction in  $D$ . Optimistically, the contribution to  $f_B$  from the  $\nu_e$  contamination in the beam might be reduced to  $\sim 0.2 - 0.5\%$  for the multi-GeV neutrino beams considered later in this report.

## 5.2 Neutral Current Backgrounds

For high energy neutrinos the NC cross section is roughly 40% of the CC cross section, and is independent of the initial flavor of the interacting neutrino. A NC interaction can result in a total visible energy anywhere from zero to the initial neutrino energy  $E_\nu$ . Some of the visible energy may be in the form of neutral pions, which can fake a single electron signature. The probability for a NC event to produce an energetic  $\pi^0$  that fakes an electron depends both on the  $\pi^0$  production rate and on the details of the detector and signal selection requirements. In the following we will begin by considering  $\pi^0$  production in NC events, and then consider various detector strategies for reducing the background.

### 5.2.1 Energetic $\pi^0$ production

Consider the probability that a NC interaction will produce an event with an energetic  $\pi^0$  that could fake a  $\nu_e$  CC interaction. Our calculations have been performed using the GEANT Monte Carlo program together with a LEPTO simulation to generate neutrino interactions [16]. A rough approximation has been used for quasi-elastic and

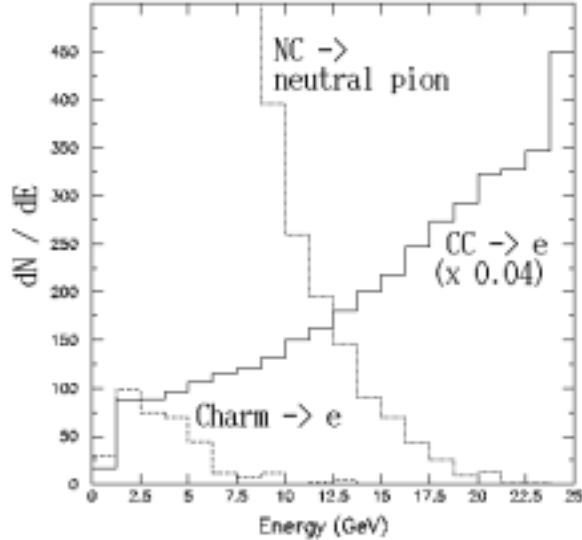


Figure 7: Energy distributions for electrons and neutral pions produced in 25 GeV neutrino interactions. Solid line: Electrons produced in CC interactions (scaled by 0.04). Dotted line: Neutral pions generated in NC interactions. Dashed line: Electrons from charm semileptonic decay.

resonance production in CC events, but no resonance production has been included for the NC events. Note that the lower the neutrino energy, the higher the fraction of quasi-elastic and resonance interactions. As a benchmark, for a 5 GeV neutrino beam the quasi-elastic and resonance contributions are about 33% of the total event rate.

The simulated energy distribution for electrons produced in 25 GeV  $\nu_e$  CC events is compared in Fig. 7 with the corresponding distribution for  $\pi^0$ 's produced in 25 GeV NC events. The  $\pi^0$  rates are small at high energy. A cut on the energy of the electron candidate can therefore reduce the NC background in a  $\nu_\mu \rightarrow \nu_e$  search. The most dangerous background events are those in which the  $\pi^0$  takes most of the energy of the hadronic fragments, and hence  $x \equiv E_{\pi^0}/E_{\text{had}}$  is large. These neutral pions can fake an isolated electron from a  $\nu_e$  CC interaction. The fraction of NC events having a  $\pi^0$  with energy greater than a given fraction of  $E_{\text{had}}$  is shown in Fig. 8 for different ranges of hadronic energy. The  $\pi^0$  fragmentation functions are roughly independent of  $E_{\text{had}}$ . To a good approximation, at large  $x$  ( $\gtrsim 0.3$ ) a single function describes all the curves shown in the figure:

$$p(x) = (0.49) - (0.96)x + (0.47)x^2 \quad (3)$$

Note that in a NC event  $E_{\text{had}}$  is just the visible energy. Within the framework of the parton model, for a given neutrino energy, the visible energy spectrum is described by [39]:

$$\frac{1}{N} \frac{dN}{dy} = \frac{15}{16} \left( 1 + \frac{(1-y)^2}{5} \right). \quad (4)$$

where  $y = E_{\text{had}}/E_\nu$ .

We can use Eqs. 3 and 4 to calculate the probability that there will be a  $\pi^0$  above some cut-off energy. Thus, for a given input neutrino energy spectrum, an output NC

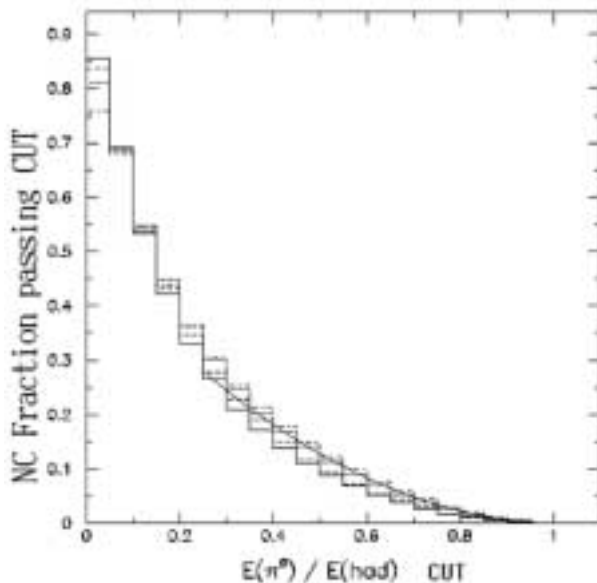


Figure 8: Fraction of NC events with a  $\pi^0$  with energy greater than a given fraction of the hadronic energy. The different histograms are for different ranges of hadronic energy: Solid:  $20 < E_{\text{had}} < 25$  GeV. Dashed:  $15 < E_{\text{had}} < 20$  GeV. Dotted:  $10 < E_{\text{had}} < 15$  GeV. Dot-Dashed:  $5 < E_{\text{had}} < 10$  GeV. The curve shows the parameterization given in the text.

background spectrum can be calculated under the assumption that all of the  $\pi^0$ 's are incorrectly identified as electrons. As an explicit example, consider a two-horn (NuMI-like) neutrino beam with a mean energy of 10 GeV, and a baseline of 9300 km (Fermilab  $\rightarrow$  SuperK), and assume the oscillation amplitude parameter  $\sin^2 2\theta_{13} = 0.01$ , and the leading oscillation scale  $\delta m_{32}^2 = 3.5 \times 10^{-3}$  eV<sup>2</sup>. The expected  $\nu_\mu \rightarrow \nu_e$  signal is compared in Fig. 9 (left panel) to various background components. In particular, the NC background spectrum is shown after requiring that the electron-candidate energy is at least 30% of the total energy, which suppresses the  $\pi^0$ 's. Note that the surviving NC background is still the dominant background component, although the others are not negligible. The total background level is about equal to the signal level for this particular example. The signal/background ratio could be improved by narrowing the energy spread of the neutrino beam. For example, if neutrinos with energies between 8 GeV and 10 GeV are selected, the right-hand panel in Fig. 9 shows the resulting signal and background distributions. Note that for this case the NC background level is roughly 1/6 of the signal.

In summary, by requiring the electron candidate to have a significant fraction of the visible event energy, the NC background can be reduced so that its contribution to  $f_B \sim 0.04$ , at the price of reducing  $D$  by  $\sim 30\%$ . Further reductions in the NC background depend on detector details, and will be discussed in the following subsections.

### 5.2.2 Liquid Argon TPC

In a liquid argon TPC there are four ways that NC events can contribute backgrounds in an electron appearance search: a) a photon converts very close to the interaction

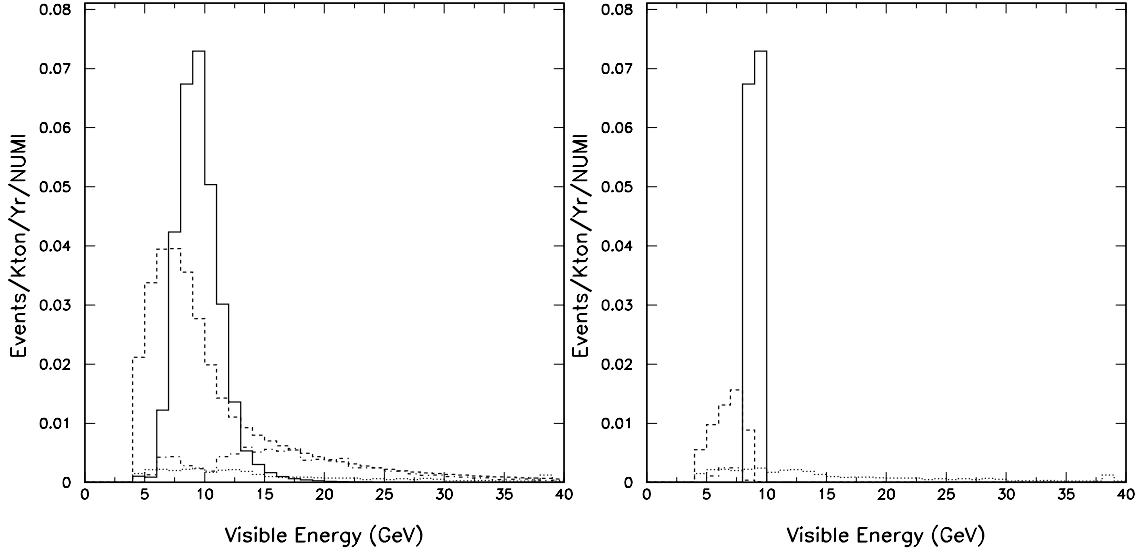


Figure 9: Differential distributions for NC,  $\nu_\tau$ , and intrinsic  $\nu_e$  backgrounds after requiring the electron candidate has at least 30% of the total event energy, compared with corresponding distributions for a  $\nu_\mu \rightarrow \nu_e$  signal ( $\sin^2 2\theta_{13} = 0.01$ ,  $\delta m_{32}^2 = 3.5 \times 10^{-3} \text{ eV}^2$ ) at  $L = 9300 \text{ km}$ . In the left panel a NuMI-like beam with a mean energy of 10 GeV is assumed. The right panel shows only the contributions from neutrinos in the beam with energies between 8 GeV and 10 GeV. Solid line: CC  $\nu_e$  signal. Dashed line: NC background. Dot-Dashed line:  $\nu_\tau$  background. Dotted line: Intrinsic  $\nu_e$  background.

vertex, b) a charged pion interacts very close to the interaction vertex, c) a charged pion overlaps with a  $\pi^0$  creating an electron-like track, or d) there is an asymmetric Dalitz decay or external conversion of a  $\pi^0$  created at the interaction vertex. The imaging capability of a liquid argon TPC of the type planned by the ICARUS collaboration is expected to facilitate much better rejection of these backgrounds than any other high-mass neutrino detector that exists or is planned.

A full simulation of the ICARUS detector [8] in the CNGS beam [17] (which has a mean neutrino energy of about 17 GeV) shows that background sources a) and d) have the largest rates, and contribute respectively 4262 and 275 out of 15550 NC events. Note that there are two charged particles resulting from the Dalitz decay or the photon conversion. These backgrounds can therefore be suppressed by requiring that the electron candidate does not have an unusually high  $dE/dx$  before it showers. Figure 10 shows an ICARUS Monte Carlo simulation of the electron/Dalitz pair separation using the first 6 cm of the “track” after the interaction vertex. Requiring the deposited energy to be less than 1 MeV would keep 90% of the signal while removing over 99% of the two-electron background. Requiring the reconstructed electron energy to exceed 1 GeV would further reduce these backgrounds by about a factor of 3. Hence, before any other kinematic or reconstruction cuts are applied, backgrounds a) and d) can be reduced to  $\sim 10^{-3}$  of the NC event rate [18].

The NC background sources b) and c), where a single charged pion either interacts or overlaps with a  $\pi^0$ , have a low rate (31.5/15550 NC events). Once again, two thirds of these events can be removed by requiring that the electron candidate has an energy greater than 1 GeV. Hence, backgrounds b) and c) can be reduced to less than  $10^{-3}$

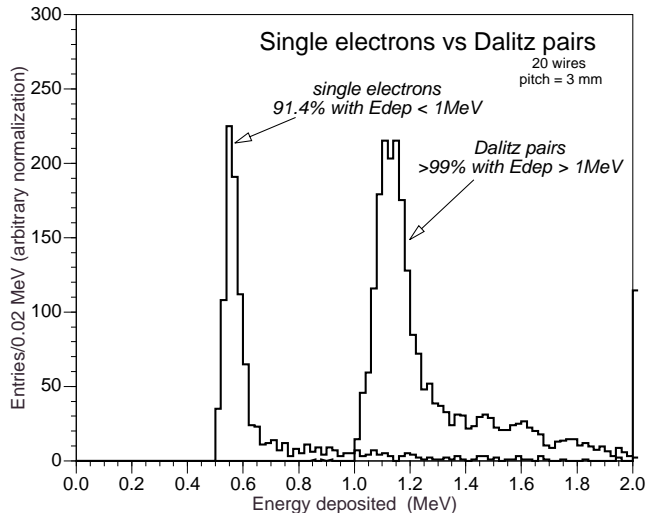


Figure 10: Simulated  $dE/dx$  measurement in liquid argon for both single electrons and Dalitz pairs based on summing over 20 wires in the ICARUS detector, or 6 cm of Liquid Argon.

of the NC event rate, at the cost of reducing  $D$  by a factor of  $\sim 0.9$ .

We conclude that, in an ICARUS-type detector, the total contribution to the background fraction  $f_B$  from NC events can be reduced to  $\sim 0.001$ , at the cost of a modest reduction in the dataset size  $D$  of  $\sim 10 - 15\%$ .

### 5.2.3 Water Cerenkov

Although Super-Kamiokande can easily discriminate between quasi-elastic  $\nu_e$  and quasi-elastic  $\nu_\mu$  events, this becomes problematic in the presence of a hadronic shower with a significant number of high energy secondaries. It was shown [4] that for neutrino energies of  $\sim 1$  GeV, the NC background contribution to  $f_B$  can be reduced to  $\sim 0.03$  at the cost of a reduction in  $D$  by a factor of 0.68. We will assume that, with further optimization,  $f_B$  can be reduced to  $\sim 0.02$ . The  $\pi^0$ 's in NC events are rejected by exploiting the cerenkov ring structure (two separated rings from  $\pi^0 \rightarrow \gamma\gamma$  decays, one ring for an electron shower). However, above neutrino energies of  $\sim 1$  GeV the two photons from the  $\pi^0$  decay are indistinguishable, and the only discrimination against NC backgrounds is based on the electromagnetic energy fraction in the event [19]. Hence we conclude that for 1 GeV neutrino beams the contribution to  $f_B$  from NC events can be reduced to about 0.02. For higher energy beams the backgrounds are much larger, and we will assume that  $f_B = 0.04$ .

### 5.2.4 Sampling Calorimeters

Sampling calorimeter neutrino detectors typically consist of a sandwich of target material (Iron, glass, Lead) and active material (scintillator or wire chambers). Relatively crude sampling calorimeters offer a compact and cost effective way of instrumenting a large fiducial mass for muon detection, and hence  $\nu_\mu$  CC measurements. However, a  $\nu_\mu \rightarrow \nu_e$  experiment requires an electron appearance measurement, which imposes significant additional requirements on the granularity of the calorimeter. In order to distinguish the electron produced in a neutrino interaction from  $\pi^0$  production,

the calorimeter must be finely segmented both longitudinally and transversely. The longitudinal segmentation is needed to resolve the difference between 1 particle (an electron) and 2 particles (from a photon conversion) at the beginning of the electromagnetic shower. The transverse segmentation is needed to prevent accidental overlaps of charged particles which would veto a real electron. We consider both fine-grained and course-grained sampling calorimeters:

- (i) Fine grained calorimeter. The Soudan 2 detector is an example of a finely segmented iron calorimeter with drift tube readout. The steel plates are 3.2 mm ( $0.18 X_0$ ) thick. The estimated fraction of NC events which fake  $\nu_e$  interactions is 2.3% after applying cuts that include requiring the candidate electron energy to be at least 50% of the visible energy. Hence, the contribution to  $f_B$  from NC events in a Soudan 2 type detector is  $\sim 0.01$ . The associated reduction in  $D$  is by a factor of 0.6.
- (ii) Course grained calorimeter. The MINOS detector is an example of a course grained iron calorimeter with scintillator readout. The toroidally magnetized steel plates are 1 inch thick, and the detector is instrumented with 4.1 cm wide scintillator strips. NC background events can be rejected based on the electron candidate energy, the total event energy, and the number of scintillator strips associated with the electron shower. A recent study [20] suggests that with the medium energy NuMI beam, the NC backgrounds for a  $\nu_\mu \rightarrow \nu_e$  search in a MINOS-like detector can be reduced so that the contribution to  $f_B$  is  $\sim 0.01$ , at the cost of reducing  $D$  by a factor of 0.33.

### 5.3 Charged Current Backgrounds

In general, in a  $\nu_\mu \rightarrow \nu_e$  search most  $\nu_\mu$  CC events can be rejected due to the presence of a muon. In our present study we only consider the  $\pi^0$  backgrounds from NC events. However, for the NuMI ME beam our simulations show that if all muons below 2 GeV in CC events are missed, the  $\pi^0$  background from CC events will roughly be equal to the corresponding background from NC events. The muon detection threshold is detector dependent, and more detailed detector studies are needed for the CC background to be taken into account.

### 5.4 Backgrounds from $\nu_\mu \rightarrow \nu_\tau$ oscillations

The oscillation process  $\nu_\mu \rightarrow \nu_\tau$  can produce a  $\nu_\mu \rightarrow \nu_e$  background if the  $\nu_\tau$  interacts to produce a tau-lepton that subsequently decays electronically ( $\tau \rightarrow e + X$ ,  $BR = 20\%$ ). If the detector does not have good discrimination between electrons and neutral pions, the process  $\tau \rightarrow n\pi^0 X \nu_\tau$  ( $BR = 37\%$ ) also contributes to the background. The  $\nu_\tau$  backgrounds are particularly dangerous because they have the same dependence on  $\delta m_{32}^2 L/E$  as the signal. Figure 11 shows the  $\nu_\tau/\nu_\mu$  CC cross section ratio as a function of neutrino energy [21]. Clearly the  $\nu_\tau$  backgrounds can be eliminated by running below, or near to, the  $\nu_\tau$  CC threshold (5 GeV).

If the neutrino beam energy is significantly above 5 GeV, one way to reduce the  $\nu_\tau$  background is to require that the electron candidate carries a significant fraction of the total observed interaction energy. Assuming a perfect detector energy resolution, the distributions of electron energy divided by total energy are shown in Fig. 12 for

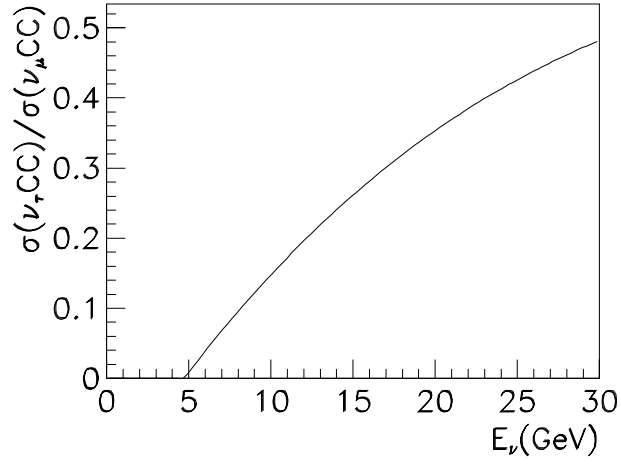


Figure 11: The  $\nu_\tau/\nu_\mu$  CC cross section ratio as a function of neutrino energy [21].

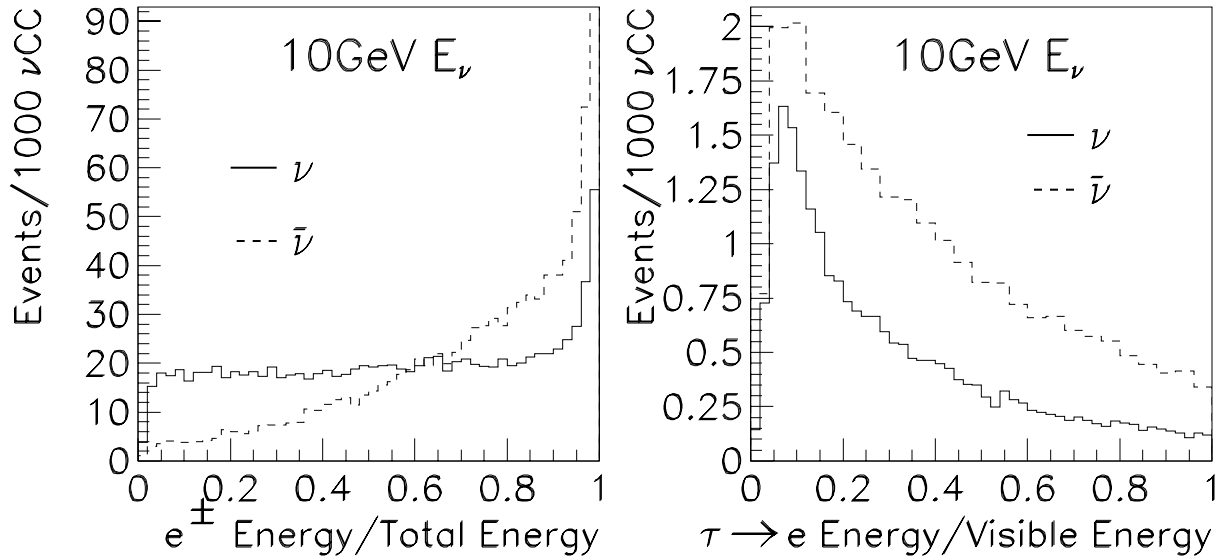


Figure 12: Ratio of electron energy to total visible energy for (left)  $\nu_e$  and  $\bar{\nu}_e$  charged current events and (right)  $\nu_\tau$  and  $\bar{\nu}_\tau$  charged current events, where the  $\tau$  subsequently decays to an electron.

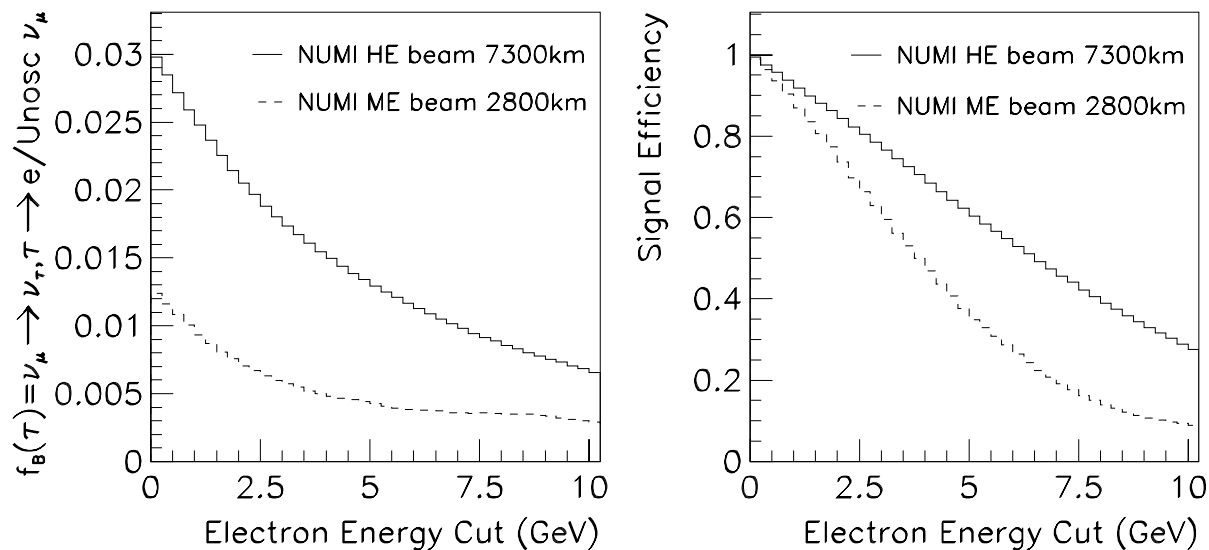


Figure 13: For oscillations with  $\delta m_{32}^2 = 3.5 \times 10^{-3} \text{ eV}^2$  and  $\sin^2 2\theta_{23} = 1$ , the  $\nu_\mu \rightarrow \nu_e$  background contribution  $f_B(\tau)$  arising  $\nu_\tau$  interactions followed by  $\tau \rightarrow e$  decays (Left panel), and the associated  $\nu_\mu \rightarrow \nu_e$  signal efficiency (right panel) shown as a function of a cut on the minimum electron energy. The energy resolution assumed for electrons is  $\sigma(E_e)/E_e = 5\%/\sqrt{E_e(\text{GeV})}$ .

10 GeV  $\nu_e$  and  $\bar{\nu}_e$  CC events (left), and 10 GeV  $\nu_\tau$  and  $\bar{\nu}_\tau$  CC events (right) where the  $\tau$  subsequently decays to an electron. If the electron candidates are required to carry at least 50% of the visible energy, the remaining  $\nu_\tau$  background level (for  $\sin^2(1.27\delta m_{32}^2 L/E) = 1$ ) is a few per cent at 10 GeV. Note that the backgrounds for  $\nu$  and  $\bar{\nu}$  running are different. Better background rejection (for a given reduction in signal efficiency) can be obtained by imposing a minimum energy requirement on the electron candidate instead of a requirement on the fraction of the total energy carried by the electron. The contribution to  $f_B$  from the  $\tau \rightarrow e + X$  backgrounds is shown in Fig. 13 as a function of the minimum electron energy requirement (left panel) for the NuMI high energy beam with  $L = 7300 \text{ km}$ , and for the medium energy beam with  $L = 2800 \text{ km}$ . The corresponding reductions in  $D$  are shown in the right panel of Fig. 13. Table 3 summarizes the expected contribution to  $f_B$  for three NuMI beams using some explicit electron energy cuts. For the medium- and high-energy beams, to reduce the contribution to  $f_B$  to  $\lesssim 0.01$  requires a significant reduction in  $D$ . Furthermore, the total contribution to  $f_B$  from  $\nu_\tau$  interactions can be a factor of  $\sim 2$  larger than listed in Table 3 if the detector does not provide adequate discrimination against  $\tau \rightarrow n\pi^0 X \nu_\tau$  decays.

There are other kinematic handles that can in principle be used to suppress  $\nu_\tau$  backgrounds, but the performance of a set of given kinematic cuts depends upon the detector details. Obvious kinematic quantities that can be exploited are the missing transverse momentum (penalizing the missing energy associated with the neutrinos produced in the  $\tau$ -lepton decay), and the electron transverse momentum distribution. The simulated distributions for these variables are shown [22] in Fig. 14 for several event types in the ICARUS detector at the CNGS beamline. Note that the CNGS beamline has

Table 3: Summary of  $\nu_\tau$  backgrounds in which  $\tau \rightarrow e + X$ . The background rates are listed for NuMI-like low-, medium-, and high-energy beams, assuming the oscillation parameters  $|\delta m_{32}^2| = 3.5 \times 10^{-3} eV^2$ , and  $\sin^2 2\theta_{23} = 1$ . The assumed electron energy resolution is  $\sigma(E_e)/E_e = 5\%/\sqrt{E_e(\text{GeV})}$ , as anticipated for the ICARUS detector. Note that the total  $\nu_\tau$  related backgrounds can be a factor of  $\sim 2$  larger if the detector does not have good discrimination against  $\tau \rightarrow n\pi^0 X\nu_\tau$  decays.

Beam	Distance (km)	$f_B(\tau)$ no cut	$f_B(\tau)$ with cut	$E_e$ cut	Signal Efficiency
NuMI-LE	732	0.001	0.001	none	1
NuMI-ME	2800	0.013	0.006	> 3 GeV	0.6
NuMI-HE	7300	0.031	0.013	> 5 GeV	0.6

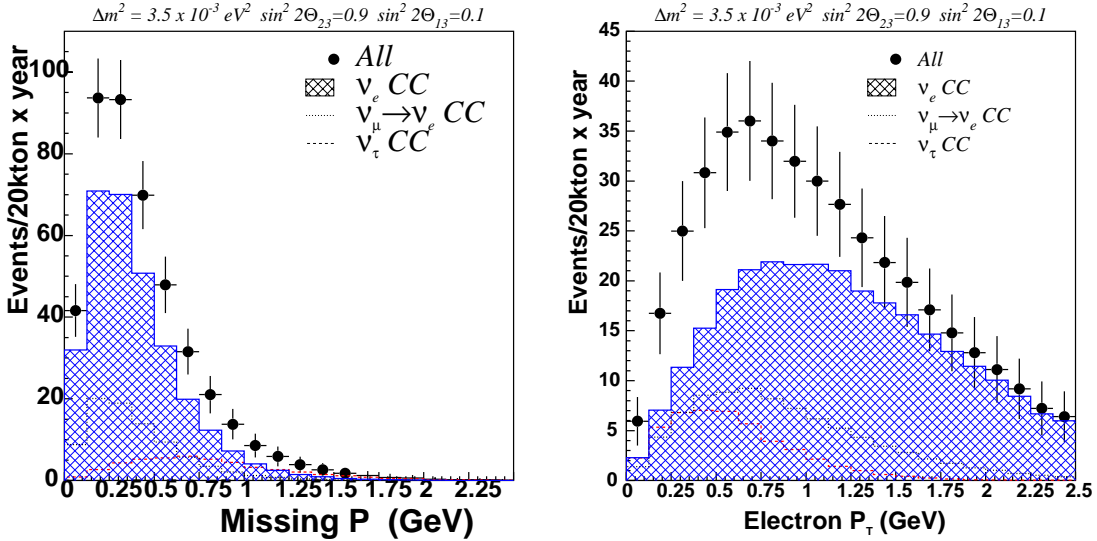


Figure 14: Missing transverse momentum (left) and electron transverse momentum (right) distributions for  $\nu_e$  charged current events and for  $\nu_\tau, \tau \rightarrow e$  events in the ICARUS detector, assuming oscillation parameters as indicated.

a  $\nu_e$  background fraction of 0.8% and a mean neutrino energy of 17 GeV, and  $\sin^2 2\theta_{13}$  has been assumed to be 0.1, just at the current limit. The distributions shown in the figure are for all electron-like events with no electron energy requirement. It should be noted that events that pass an electron energy cut will tend to have electrons moving close to the  $\nu_\tau$  direction, and hence are more likely to survive other kinematic cuts. For an experiment in which the  $\tau$  appearance rate is likely to be significant, the ICARUS collaboration finds the best sensitivity is obtained with a combined fit, rather than by eliminating the  $\nu_\tau$  events.

We conclude that  $\nu_\tau$  backgrounds are only significant for the medium- and high-energy beams, in which case an electron energy cut and/or good  $\tau \rightarrow e$  rejection is needed to reduce the contribution to  $f_B$  to  $\lesssim 0.01$ . This might be accomplished in a liquid argon detector, which provides good discrimination against  $\tau \rightarrow n\pi^0 X\nu_\tau$  decays. The  $\tau$  related backgrounds might be larger in other detectors. For example, a recent study [20] concluded that, with  $\delta m_{32}^2 = 0.003 \text{ eV}^2$  and  $L = 2900 \text{ km}$ , after cuts which reduced  $D$  by a factor of 0.33, the contribution to  $f_B$  from  $\nu_\mu \rightarrow \nu_\tau$  associated interactions was 0.02 for a MINOS-like iron-scintillator detector at a NuMI-like medium energy beam.

## 5.5 The systematic uncertainty on the background

Since a  $\nu_\mu \rightarrow \nu_e$  search will not be background free, the background must be subtracted from any potential signal. The background subtraction introduces a systematic uncertainty associated with the imperfect knowledge of the expected background rate. Assigning a systematic error on the background rate requires understanding the uncertainty on the  $\nu_e$  contamination in the beamline, and the uncertainty on the detector's ability to reject background events.

To understand the  $\nu_e$  fraction in the initial neutrino beam, we must know the charged and neutral kaon components in the secondary beam. This requires knowledge of their production at the proton target, and knowledge of the beamline acceptance. In addition, the backgrounds from muons decaying in the decay tunnel must be understood, although generally speaking the uncertainty from this background component is relatively small. Measuring the fraction of charged and neutral kaons produced in the target is the subject of much current study. The experiment P907 [23] is being proposed at Fermilab to measure the kaon production cross sections for 120 GeV protons on the MINOS target. A similar experiment, HARP [24], is planned at CERN to study meson production for the CNGS beam. P907 and HARP are expected to significantly reduce the kaon production uncertainties for neutrino beams using 120 GeV and multi-GeV (up to 15 GeV) proton beams, together with targets similar to NuMI and CNGS. However, the combined effects of both production and acceptance must be understood. For this purpose, a very fine-grained near detector could be used. As an example, the NOMAD detector [25] can determine the neutral kaon contribution to the  $\nu_e$  flux by comparing the rates of  $\nu_e$  and  $\bar{\nu}_e$  events that are seen. With an electron charge analysis to discriminate between  $\nu_e$  and  $\bar{\nu}_e$  events, the NOMAD experiment is able to limit the systematic uncertainty on the overall near detector  $\nu_e$  flux to 2%, and the energy spectrum shape to 2.5% [26]. With a fine-grained near detector of this type one might imagine achieving a systematic uncertainty on the far detector flux of 3 to 4%.

Background rejection in the far detector can be understood using a second near

detector of the same type as the far detector, Assuming that appropriate near detectors are used, the remaining systematic uncertainties on the backgrounds in the far detector come from the slightly different beam spectrum that any near detector sees, and the uncertainties on the differences in fiducial volumes and event acceptances. While there is probably no hard limit on the systematic uncertainty that could be achieved, it is unreasonable to expect that the total systematic uncertainty on the background fraction could be reduced below a few per cent of the background itself. In the following we will assume that the uncertainty on the background rates is 5%. Note that the participants of a recent study of 1 GeV neutrino beams at the JHF [4] assumed the more conservative value of 10% for the systematic uncertainty on the backgrounds.

## 5.6 Summary: Dataset size $D$ & background fraction $f_B$

In the previous discussion we concluded that, for a  $\nu_\mu \rightarrow \nu_e$  measurement, the contribution to the expected background fraction  $f_B$  from the initial  $\nu_e$  beam contamination might be reduced to  $\sim 0.002$ . However, for most of the detector types we have considered,  $f_B$  is dominated by the contributions from (a) neutral pions faking an electron signature, and/or (b)  $\nu_\mu \rightarrow \nu_\tau$  related backgrounds. We would like to know, as a function of detector choice, the values of  $f_B$  and  $D$  that should be used in assessing the  $\nu_\mu \rightarrow \nu_e$  physics potential. The dominant contributions to  $f_B$ , together with  $f_B$  and the associated signal efficiencies, and detector cost estimates, are summarized in Table 4, along with the implied value of  $D$  for 5 years of data taking. The values of  $D$  are estimated assuming the detectors cost \$500M, which determines the detector masses. Estimating the unit costs for each detector type is not straightforward. Details of the cost estimates are given in Appendix 2.

Note that no detector achieves the goal  $f_B < 0.004$  that we derived in Section 4 for a multi-GeV beam. Once above the  $\nu_\tau$  CC threshold the contribution to  $f_B$  from  $f_B(\tau)$  already exceeds 0.004. As an example, consider the liquid Argon detector. The parameters to be used for this detector type with a medium energy MINOS-type beam are:  $D = 170$  kt-yrs,  $f_B = 0.008$ , and  $\sigma_{f_B}/f_B = 0.05$  (as discussed in Section 5.5). If the  $\nu_\tau$  background contribution could be eliminated  $f_B$  would be reduced to  $\sim 0.003$ , but this improvement in background rate would be accompanied by a significant decrease in  $D$ , and would not be expected to significantly improve the sensitivity to  $\nu_\mu \rightarrow \nu_e$  oscillations.

## 6 Physics with multi-GeV long-baseline beams

Using the values of  $D$  and  $f_B$  in Table 4, and assuming  $\sigma_{f_B}/f_B = 0.05$ , we can now assess the physics potential for the various detector scenarios we have considered. We will begin with the multi-GeV long baseline beams, and consider the minimum value of  $\sin^2 2\theta_{13}$  that will yield a  $\nu_\mu \rightarrow \nu_e$  signal  $3\sigma$  above the background, the sensitivity to the neutrino mass hierarchy, and the sensitivity to CP violation in the lepton sector.

### 6.1 $\sin^2 2\theta_{13}$ Reach

To obtain the  $\sin^2 2\theta_{13}$  reach for the detector scenarios listed in Table 4 we return to Fig. 5 which shows contours of constant reach in the  $(f_B, D)$ -plane for upgraded

Table 4: Detector background rates ( $f_B$ ), signal efficiencies, and unit costs. Water cerenkov backgrounds and efficiencies are neutrino energy dependent: numbers left of the arrows for a 1 GeV beam, numbers right of the arrows for a multi-GeV beam requiring  $y < 0.5$ .

	Water Cerenkov (UNO)	Liquid Argon (ICARUS)	Steel+readout (MINOS) (THESEUS)		Liquid <sup>f</sup> Scintillator
Signal Efficiency	0.7 → 0.5	0.90	0.33	0.6 <sup>b, g</sup>	0.76
$f_B(\text{NC})$	0.02 → 0.04	0.001	0.01	0.01	< 0.006
$f_B(\text{beam})$	0.002	0.002	0.002	0.002	0.002
$f_B(\tau)$	0 → 0.01	~ 0.005 <sup>c</sup>	0.02 <sup>c</sup>	0 <sup>b</sup>	~ 0.005 <sup>c</sup>
$f_B$	0.02 → 0.05	~ 0.008	0.03	0.01	~ 0.01
Electron cut	> 0.5 × $E_\nu$	none <sup>d</sup>	1-6 GeV	> 0.5 $E_{vis}$	$E_{vis} > 2$ GeV
Unit cost (M\$/kt) <sup>a</sup>	2.4	23	10.4	78	59
Mass (kt) / 500 M\$	745	37	85	6.4	260
$D$ (kt-yrs) <sup>e</sup>	2600 → 1860	170	140	19	990

<sup>a</sup> FY00 dollars. Costs account for salaries, overheads, and contingencies. Details are given in Appendix 2. The cost does not include excavating a cavern, which is estimated [27] to be 0.5M\$/kton/ $\rho$ , ( $\rho$  = target density).

<sup>b</sup> For the MINOS low energy beam.

<sup>c</sup> For the MINOS medium energy beam.

<sup>d</sup> Although a total energy cut might be applied to reduce the intrinsic  $\nu_e$  background.

<sup>e</sup> For 5 years running.

<sup>f</sup>  $\nu_e n \rightarrow e^- p$  search, Ahrens et al, Phys. Rev. D volume 36, (702) 1987.

<sup>g</sup> Soudan efficiency for electron neutrinos: NuMI-L-562.

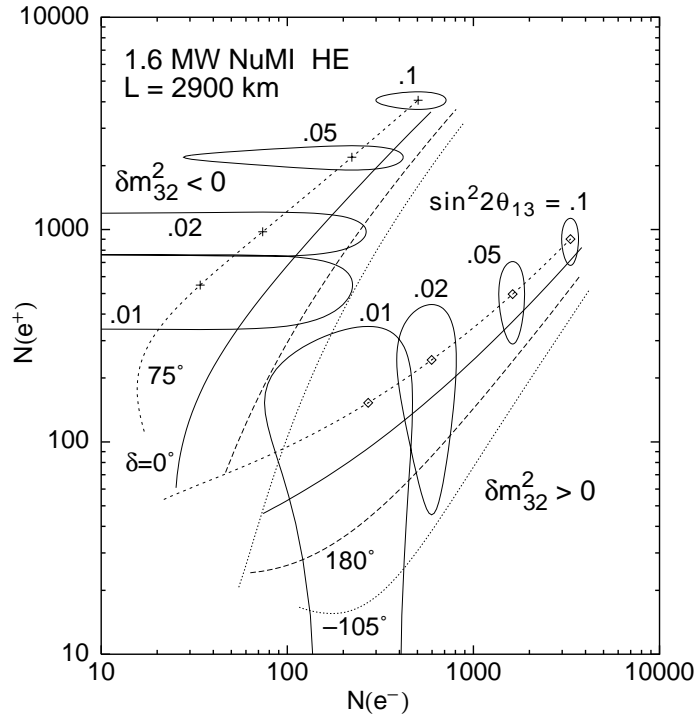


Figure 15: Three-sigma error ellipses in the  $(N(e^+), N(e^-))$ -plane, shown for  $\nu_\mu \rightarrow \nu_e$  and  $\bar{\nu}_\mu \rightarrow \bar{\nu}_e$  oscillations in a NuMI-like high energy neutrino beam driven by a 1.6 MW proton driver. The calculation assumes a liquid argon detector with the parameters listed in Table 4, a baseline of 2900 km, and 3 years of running with neutrinos, 6 years running with antineutrinos. Curves are shown for different CP-phases  $\delta$  (as labelled), and for both signs of  $\delta m_{32}^2$  with  $|\delta m_{32}^2| = 0.0035 \text{ eV}^2$ , and the sub-leading scale  $\delta m_{21}^2 = 10^{-4} \text{ eV}^2$ . Note that  $\sin^2 2\theta_{13}$  varies along the curves from 0.0001 to 0.01, as indicated [13].

(1.6 MW) NuMI medium- and high-energy beams. Of the scenarios we have considered, the greatest sensitivity is obtained using a liquid argon detector with either the medium- or high-energy beams at  $L = 2900 \text{ km}$ ,  $4000 \text{ km}$ , or  $7300 \text{ km}$ . In these cases a  $\nu_\mu \rightarrow \nu_e$  signal at least  $3\sigma$  above the background would be expected provided  $\sin^2 2\theta_{13} > 0.002$  to  $0.003$ . If the  $\nu_\tau$  backgrounds could be eliminated, reducing  $f_B$  to  $0.003$ , the limiting sensitivity improves to  $\sin^2 2\theta_{13} > 0.001$ . If the initial  $\nu_e$  contamination in the beam is  $0.5\%$  (rather than the assumed  $0.2\%$ ), so that  $f_B = 0.01$ , the  $\sin^2 2\theta_{13}$  reach is still  $\sim 0.002$  to  $0.003$ . Hence, the estimated reach is not very sensitive to the uncertainties on our background estimations. However, the  $\nu_\mu \rightarrow \nu_e$  sensitivity would be degraded if the  $\nu_\tau$  backgrounds were significantly larger, which disfavors higher beam energies.

We conclude that, with a 30-40 kt liquid argon detector and a medium energy superbeam, we could improve the sensitivity to  $\nu_\mu \rightarrow \nu_e$  oscillations, and obtain about an order of magnitude improvement in the  $\sin^2 2\theta_{13}$  reach beyond that expected for the currently approved next generation experiments. The other detector choices in Table 4 do not seem to be competitive with liquid argon, with the possible exception of the water cerenkov detector which obtains a reach of about  $0.003$  with the high energy beam at the longest baseline ( $L = 7300 \text{ km}$ ).

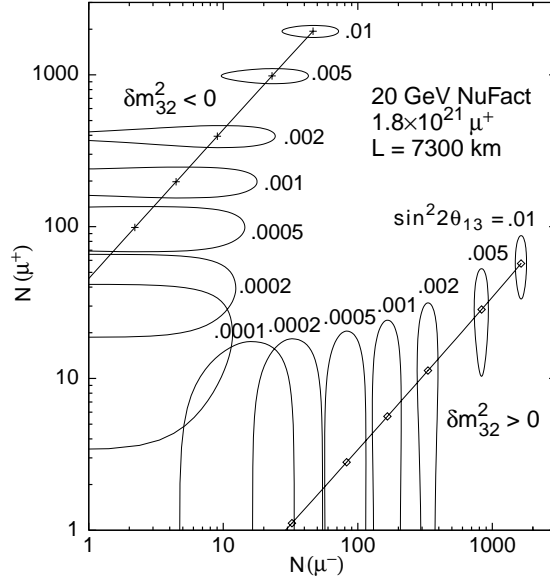


Figure 16: Three-sigma error ellipses in the  $(N(\mu+), N(\mu-))$ -plane, shown for a 20 GeV neutrino factory delivering  $3.6 \times 10^{21}$  useful muon decays and  $1.8 \times 10^{21}$  antimuon decays, with a 50 kt detector at  $L = 7300$  km,  $\delta m_{21}^2 = 10^{-4}$  eV<sup>2</sup>, and  $\delta = 0$ . Curves are shown for both signs of  $\delta m_{32}^2$ ;  $\sin^2 2\theta_{13}$  varies along the curves from 0.0001 to 0.01, as indicated [13].

## 6.2 Matter Effects and CP Violation

Having either established or excluded a  $\nu_\mu \rightarrow \nu_e$  signal, a search for  $\bar{\nu}_\mu \rightarrow \bar{\nu}_e$  over a long baseline can determine the sign of  $\delta m_{32}^2$ , and hence the neutrino mass hierarchy. Suppose that  $N_+$  and  $N_-$  signal events are measured in neutrino and antineutrino running respectively. In the absence of intrinsic CP-violation, and in the absence of matter effects, after correcting for different beam fluxes, experimental livetimes, and the neutrino/antineutrino cross section ratio, we would expect  $N_+ = N_-$ . However, if  $\delta m_{32}^2 > 0$ , matter effects can reduce  $N_+$  and enhance  $N_-$ . Alternatively, if  $\delta m_{32}^2 < 0$ , matter effects can reduce  $N_-$  and enhance  $N_+$ . For detector scenarios and multi-GeV beams similar to those considered in this report, it has been shown [13] that:

- (i) At  $L = 732$  km the expected changes of  $N_+$  and  $N_-$  due to matter effects are modest, and are comparable to changes that might arise with maximal CP-violation in the lepton sector. It is therefore difficult to observe and disentangle matter from CP effects unless the baseline is longer.
- (ii) At baselines of  $\sim 3000$  km or greater matter effects are much larger than CP effects, and the determination of the sign of  $\delta m_{32}^2$  is straightforward provided both  $N_+$  and  $N_-$  have been measured with comparable sensitivities, and at least one of them is non-zero. The sign of  $\delta m_{32}^2$  can be determined with a significance of at least  $3\sigma$  provided  $\sin^2 2\theta_{13} \gtrsim 0.01$ .
- (iii) CP violation cannot be unambiguously established in any of the long baseline scenarios considered.

To illustrate these points we choose one of the most favorable scenarios studied: a 1.6 MW NuMI-like high energy beam with  $L = 2900$  km, detector parameters  $f_B$  and

$D$  corresponding to the liquid argon scenario in Table 4, and oscillation parameters  $|\delta m_{32}^2| = 3.5 \times 10^{-3} \text{ eV}^2$  and  $\delta m_{21}^2 = 1 \times 10^{-4} \text{ eV}^2$ . The calculated three-sigma error ellipses in the  $(N(e^+), N(e^-))$ -plane are shown in Fig. 15 for both signs of  $\delta m_{32}^2$ , with the curves corresponding to various CP-phases  $\delta$  (as labelled). The magnitude of the  $\nu_\mu \rightarrow \nu_e$  oscillation amplitude parameter  $\sin^2 2\theta_{13}$  varies along each curve, as indicated. The two groups of curves, which correspond to the two signs of  $\delta m_{32}^2$ , are separated by more than  $3\sigma$  provided  $\sin^2 2\theta_{13} \gtrsim 0.01$ . Hence the mass hierarchy can be determined provided the  $\nu_\mu \rightarrow \nu_e$  oscillation amplitude is not less than an order of magnitude below the currently excluded region. Unfortunately, within each group of curves, the CP-conserving predictions are separated from the maximal CP-violating predictions by at most  $3\sigma$ . Hence, it will be difficult to conclusively establish CP violation in this scenario.

Note for comparison that a very long baseline experiment at a neutrino factory would be able to observe  $\nu_e \rightarrow \nu_\mu$  oscillations and determine the sign of  $\delta m_{32}^2$  for values of  $\sin^2 2\theta_{13}$  as small as  $O(0.0001)$ ! This is illustrated in Fig. 16.

## 7 Physics with 1 GeV medium baseline beams

We next turn our attention to neutrino beams with energy  $E_\nu \sim 1 \text{ GeV}$ . The atmospheric neutrino deficit scale  $\delta m_{32}^2$  then sets a baseline requirement  $L \sim 300 \text{ km}$ . A recent study [4] has generated a letter of interest for a 1 GeV neutrino beam at the Japan Hadron Facility (0.77 MW 50 GeV proton driver), with a baseline of 295 km, using the SuperK detector [31]. The JHF study group has considered a variety of beamline designs, including both narrow band and wide band beams, quadrupole and horn based focusing. The energy distributions for these beams are shown in Fig. 17 (left panel). With a water cerenkov detector the JHF group finds that for a  $\nu_\mu \rightarrow \nu_e$  search it is important to use a narrow band beam to avoid the high energy neutrino tail which provides a significant source of high energy NC events with detected neutral pions that fake lower energy electrons. With a narrow band beam, after detailed studies of signal efficiency and background rejection they obtain  $f_B = 0.03$ , dominated by the surviving NC backgrounds. This background level was obtained at the cost of reducing  $D$  by a factor of 0.68. The initial  $\nu_e$  component in the beam contributes only 0.004 to  $f_B$ . An uncertainty on the background rates of 10% was assumed.

In the following we discuss the sensitivity of a 1 GeV medium baseline neutrino beam to  $\nu_\mu \rightarrow \nu_e$  oscillations, and the prospects for observing CP-violation. Note that baselines of a few hundred kilometers are too short for matter effects to be appreciable, and hence the pattern of neutrino masses cannot be determined with these medium baseline beams.

### 7.1 $\sin^2 2\theta_{13}$ reach

The JHF study group concluded that, if no  $\nu_e$  appearance signal was observed after 5 years of running, taking the central SuperK value for  $\delta m_{32}^2$ , they would be able to exclude  $\nu_\mu \rightarrow \nu_e$  oscillation amplitudes greater than 0.01 at 90% C.L., which is about an order of magnitude better than the present limit (Fig. 17 right panel). This level of sensitivity corresponds to a  $\sin^2 2\theta_{13}$  reach of  $\sim 0.03$ . With a larger dataset (20 times SuperK) the reach is improved by about a factor of 4.

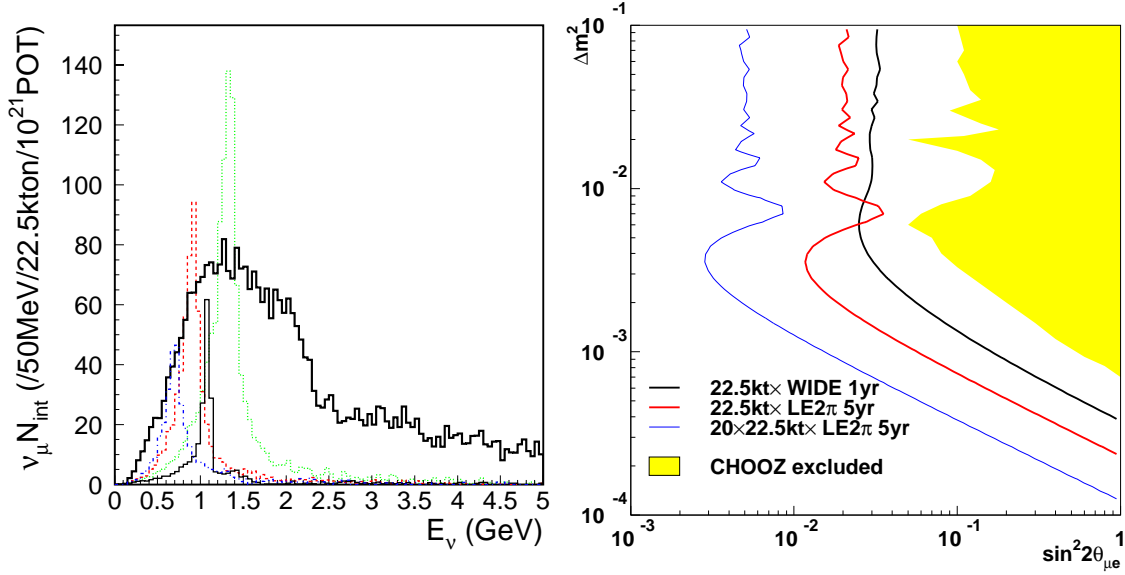


Figure 17: Differential event rates (left) and two-flavor  $\nu_\mu \rightarrow \nu_e$  oscillation sensitivity (right) for a 1 GeV neutrino beam at the JHF with  $L = 295$  km, and a water cerenkov detector. In the left panel the thick solid histogram is for a wide band beam, and the thin solid, dashed, dotted, and dot-dash histograms are for four narrow band beam designs. The 90% C.L. contours in the right panel are for, as indicated, 1 year with a wide band beam, 5 years with a narrow band beam and the SuperK detector, and 5 years with a narrow band beam and  $20 \times$  the SuperK detector [4].

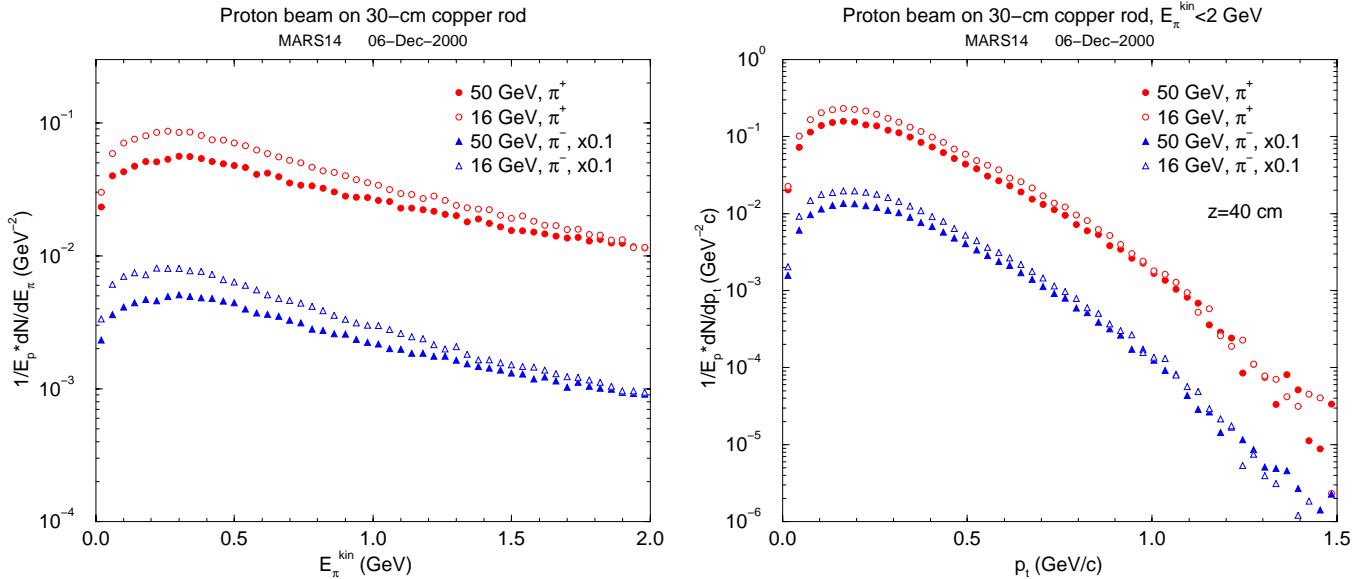


Figure 18: Charged pion production for 16 GeV and 50 GeV protons incident on a 30 cm copper target. The  $\pi^+$  and  $\pi^-$  kinetic-energy (left) and transverse momentum (right) spectra are shown for forward going particles within a cone of angle 1 radian. To facilitate a comparison at equal beam power the rates have been divided by the incident proton energy. For clarity, the  $\pi^-$  spectra have been scaled down by an additional factor of 10.

It is interesting to see where the JHF scenario lies in the  $(f_B, D)$ -plane shown in Fig. 4. If we take  $f_B = 0.03$  and  $D = 77$  kt-years (5 years of data taking in the superK detector with a signal efficiency of 0.68), we see that the JHF  $\rightarrow$  SuperK scenario lies close to the  $\sin^2 2\theta_{13} = 0.03$  contour. Thus the calculations of Ref. [13] are in agreement with the JHF study group results. Note that the JHF scenario already lies in the background systematics dominated (vertical contour) region of the plane. Upgrading the detector mass by a large factor only results in a modest improvement in the  $\sin^2 2\theta_{13}$  reach. With  $D = 2600$  kt-years and  $f_B = 0.02$ , the reach has improved to  $\sin^2 2\theta_{13} \sim 0.01$  at the 0.77 MW JHF. It is unclear whether an upgraded 4 MW JHF would further improve the reach, which is very sensitive to  $\sigma_{f_B}/f_B$  in the systematics dominated region of the  $(f_B, D)$ -plane. A liquid argon detector, with  $f_B = 0.003$ ,  $\sigma_{f_B}/f_B = 0.05$ , and  $D = 170$  kt-years, would obtain a reach of  $\sim 0.01$  at the 0.77 MW JHF, and  $\sim 0.003$  at an upgraded 4 MW JHF.

To a good approximation we would expect the JHF study results to apply also to a 1 GeV neutrino beam generated at Fermilab using a 16 GeV  $\sim 1$  MW proton driver. Charged pion production spectra for 16 GeV and 50 GeV protons are compared in Fig. 18, with the spectra normalized by dividing by the proton beam energies. Hence the pion event rates are shown at equal beam powers. The shapes of the 16 GeV and 50 GeV kinetic energy- and transverse-momentum-distributions are similar. At equal beam power, the sub-GeV pion rates obtained with 16 GeV protons are approaching a factor of two higher than the 50 GeV rates. Above 1 GeV the rates obtained with 16 GeV protons are similar to those obtained with 50 GeV protons if the beam powers are similar. Hence we would expect the 1 GeV neutrino beam fluxes at the JHF to be similar to the fluxes at an  $\sim 1$  MW 16 GeV machine.

## 7.2 Searching for CP-violation

If  $\sin^2 2\theta_{13}$  lies within an order of magnitude of the present experimental limits, we would expect a  $\nu_\mu \rightarrow \nu_e$  signal to be established in either the next generation of accelerator based neutrino experiments, or at a future superbeam experiment. In this case, if the solar neutrino deficit is correctly described by the LMA MSW solution there is the tantalizing possibility of observing CP-violation in the lepton sector, and measuring the CP-violating amplitude. In a medium baseline experiment the CP-violating signature (an asymmetry between the  $\nu_\mu \rightarrow \nu_e$  and  $\bar{\nu}_\mu \rightarrow \bar{\nu}_e$  oscillation probabilities) is not complicated by matter effects, which are very small.

Consider the sensitivity to CP-violation at the JHF with  $L = 295$  km. Both the background levels and the associated systematic uncertainty are expected to be worse for antineutrino beams than for neutrino beams. In the following, for simplicity we will consider backgrounds and systematics to be the same for  $\nu$  and  $\bar{\nu}$  beams, and take  $f_B = 0.02$  and  $\sigma_{f_B}/f_B = 0.1$ . Figure 19 shows the expected sensitivity to maximal CP-violation ( $\delta = 90^\circ$ ) after 3 years of neutrino running to measure the number of  $\nu_\mu \rightarrow \nu_e$  events, followed by 6 years of antineutrino running to measure the number of  $\bar{\nu}_\mu \rightarrow \bar{\nu}_e$  events. In the absence of CP-violation we would expect the two signal samples to have the same number of events on average since the factor of two difference in neutrino and antineutrino cross-sections is compensated by the difference in the running times. Hence the broken curves at  $45^\circ$  in the figure correspond to the CP-conserving case. The figure shows  $3\sigma$  error ellipses for a water cerenkov detector with a fiducial mass of 220 kt at the 0.77 MW JHF (left panel), and a liquid argon TPC with a fiducial mass of 30 kt

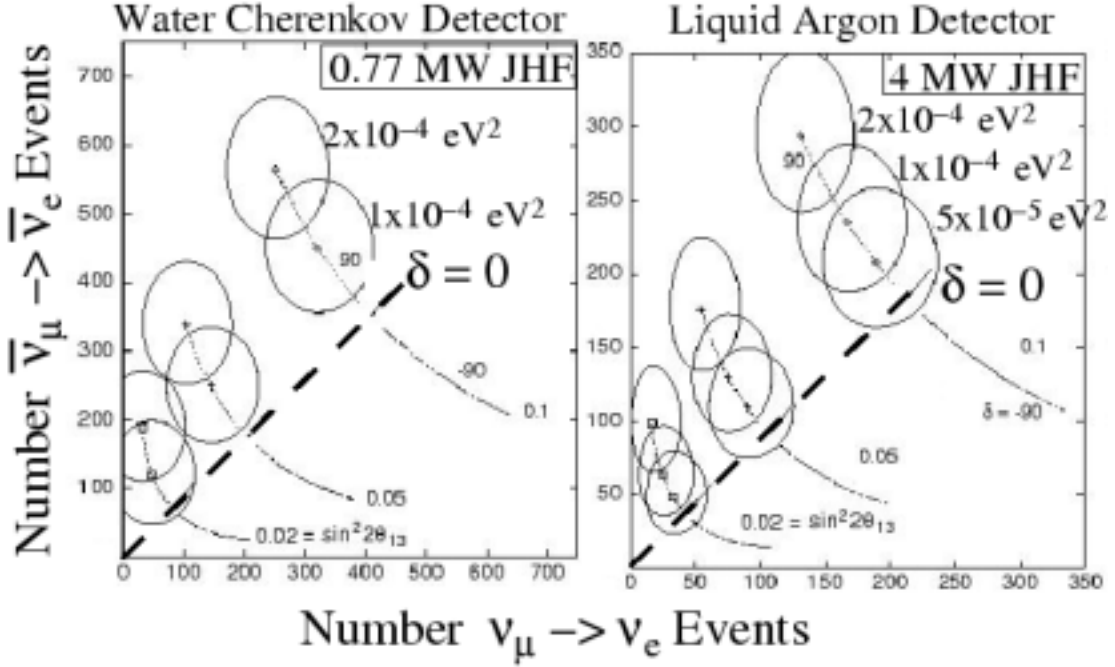


Figure 19: Three-sigma error ellipses in the  $(N_+, N_-)$ -plane, where  $N_-$  is the number of  $\nu_\mu \rightarrow \nu_e$  signal events and  $N_+$  is the number of  $\bar{\nu}_\mu \rightarrow \bar{\nu}_e$  signal events, shown for 1 GeV neutrino beams with  $L = 295$  km at the 0.77 MW JHF using a 220 kt water cerenkov detector (left panel) with  $f_B = 0.02$ , and at the 4 MW upgraded JHF with a 30 kt liquid argon detector (right panel) with  $f_B = 0.004$ . The 3 families of ellipses correspond to  $\sin^2 2\theta_{13} = 0.02, 0.05,$  and  $0.1$ , as labelled. The solid (dashed) [dotted] curves correspond to  $\delta = 0^\circ$  ( $90^\circ$ ) [ $-90^\circ$ ] with  $\delta m_{21}^2$  varying from  $2 \times 10^{-5}$  eV $^2$  to  $2 \times 10^{-4}$  eV $^2$ . The error ellipses are shown on each curve for  $\delta m^2 = 5 \times 10^{-5}, 10^{-4}$  and  $2 \times 10^{-4}$  eV $^2$ . The curves assume 3 years of neutrino running followed by 6 years of antineutrino running [13].

at a 4 MW upgraded JHF (right panel). The error ellipses are shown for three different sub-leading scales  $\delta m_{21}^2 = 2 \times 10^{-4}, 1 \times 10^{-4},$  and  $5 \times 10^{-5}$  eV $^2$ . In each panel the three families of ellipses correspond to three values of  $\sin^2 2\theta_{13}$ . Note that parameter values with ellipses that lie entirely above the  $\delta = 0$  line would result in a  $3\sigma$  observation of maximal CP-violation. We see that for the water cerenkov scenario, if  $\sin^2 2\theta_{13} = 0.1$ , marginally below the currently excluded region, then maximal CP-violation would be observed provided  $\delta m_{21}^2$  is not significantly below  $1 \times 10^{-4}$  eV $^2$ , which is at the upper end of the preferred solar neutrino deficit LMA region. The sensitivity is only marginally better in the liquid argon scenario. With decreasing  $\sin^2 2\theta_{13}$  the sensitivity slowly decreases, with  $1 \times 10^{-4}$  eV $^2$  being the limiting  $\delta m_{21}^2$  for  $\sin^2 2\theta_{13} \sim 0.02$ . Hence, for a small region of presently favored MSW LMA parameter space, maximal CP Violation could be seen at  $3\sigma$  at a 1 GeV medium baseline superbeam. This small exciting piece of parameter space can be described approximately by:

$$\sin^2 2\theta_{13} > 0.02, \quad \sin \delta \times \delta m_{21}^2 > 7 \times 10^{-5} \text{ eV}^2 \quad (5)$$

## 8 Conclusions

Neutrino superbeams that exploit MW-scale proton drivers, together with detectors that are an order of magnitude larger than those presently foreseen, offer the prospect of improving the sensitivity to  $\nu_\mu \rightarrow \nu_e$  oscillations by an order of magnitude beyond the next generation of experiments. Superbeams would therefore provide a useful tool en route to a neutrino factory. Our main conclusions are:

- (i) We believe that the initial  $\nu_e$  contamination in the beam might be reduced to  $\sim 0.2\%$ , although we note that the contributions from  $K_L$  decay will make this goal difficult to achieve for multi-GeV beams.
- (ii) The dominant  $\nu_\mu \rightarrow \nu_e$  backgrounds will arise from (a)  $\pi^0$  production in NC events, where the  $\pi^0$  subsequently fakes an electron signature, and (b)  $\nu_\tau$  CC interactions (if the beam energy is above  $\sim 5$  GeV).
- iii) Of the detector technologies we have considered, only the liquid argon detector offers the possibility of reducing the background fraction  $f_B$  significantly below 0.01. A multi-GeV long baseline superbeam experiment with a liquid argon (water cerenkov) detector would be able to observe a  $\nu_\mu \rightarrow \nu_e$  signal with a significance of at least  $3\sigma$  above the background provided  $\sin^2 2\theta_{13} \gtrsim 0.002 - 0.003$  (0.003). If the baseline  $L \gtrsim 3000$  km, the same experiment would also be able to determine the sign of  $\delta m_{32}^2$  provided  $\sin^2 2\theta_{13} \gtrsim 0.01$ . However, it seems unlikely that an unambiguous signal for CP-violation could be established with a multi-GeV superbeam.
- (iv) A 1 GeV medium baseline superbeam experiment with a liquid argon detector would be able to observe a  $\nu_\mu \rightarrow \nu_e$  signal with a significance of at least  $3\sigma$  above the background provided  $\sin^2 2\theta_{13} \gtrsim 0.003$ . The experiment would not be able to determine the sign of  $\delta m_{32}^2$ , but if the LMA MSW solution correctly describes the solar neutrino deficit, there is a small region of allowed parameter space for which CP-violation in the lepton sector might be established.

We compare the superbeam  $\nu_\mu \rightarrow \nu_e$  reach with the corresponding neutrino factory  $\nu_e \rightarrow \nu_\mu$  reach in Fig. 20, which shows the  $3\sigma$  sensitivity contours in the  $(\delta m_{21}^2, \sin^2 2\theta_{13})$ -plane. The superbeam  $\sin^2 2\theta_{13}$  reach of a few  $\times 10^{-3}$  is almost independent of the sub-leading scale  $\delta m_{21}^2$ . However, since the neutrino factory probes oscillation amplitudes  $O(10^{-4})$  the sub-leading effects cannot be ignored, and a signal would be observed at a neutrino factory over a significant range of  $\delta m_{21}^2$  even if  $\sin^2 2\theta_{13} = 0$ .

Finally, both the possibility of exploiting sub-GeV superbeams (not considered in our present study), and the optimum detector designs for GeV and multi-GeV experiments, deserve further consideration.

### Acknowledgments

We would like to acknowledge support for this study from the U.S. Department of Energy, the Illinois Dept. of Commerce and Community Affairs, the Illinois State Board of Higher Education, and the National Science Foundation.

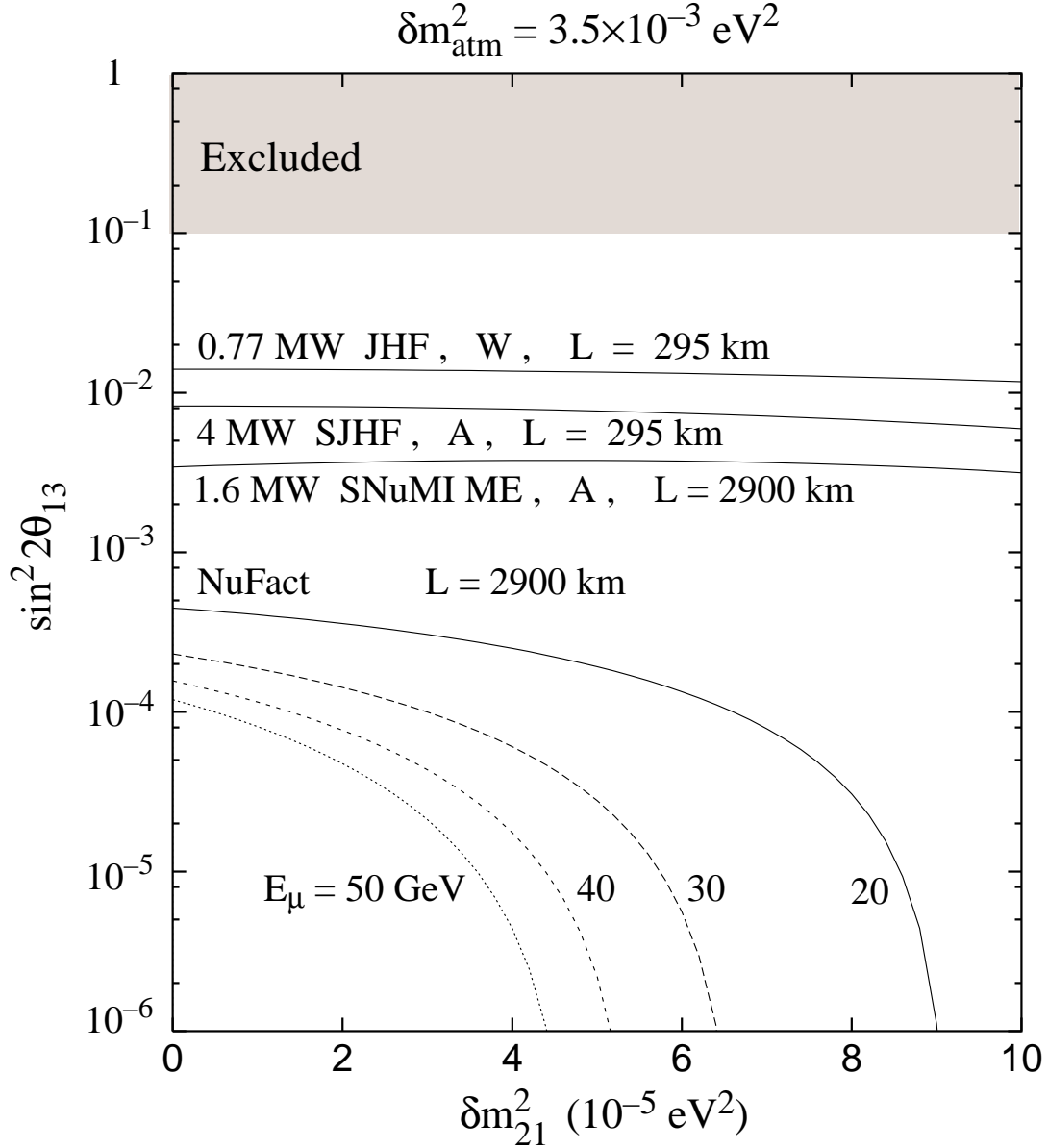


Figure 20: Summary of the  $3\sigma$  level sensitivities for the observation of  $\nu_\mu \rightarrow \nu_e$  at various MW-scale superbeams (as indicated) with liquid argon “A” and water cerenkov “W” detector parameters, and the observation of  $\nu_e \rightarrow \nu_\mu$  in a 50 kt detector at 20, 30, 40, and 50 GeV neutrino factories delivering  $2 \times 10^{20}$  muon decays in the beam forming straight section. The limiting  $3\sigma$  contours are shown in the  $\delta m_{21}^2, \sin^2 2\theta_{13}$ -plane. All curves correspond to 3 years of running. The grey shaded area is already excluded by current experiments.

## References

- [1] C. Albright et al., “Physics at a Neutrino Factory”, report to the Fermilab Directorate, FERMILAB-FN-692, April 2000.
- [2] S. Geer, Phys. Rev. **D57**, 6989 (1998).
- [3] N. Holtkamp, D.A. Finley, *et al*, FERMILAB-PUB-00-108-E, June 2000, submitted to Phys.Rev.ST Accel.Beams.
- [4] Y. Itow *et al*, Japanese Hadron Facility Letter of Intent, February 2000.
- [5] K. Nishikawa et al. (KEK-PS E362 Collab.), “Proposal for a Long Baseline Neutrino Oscillation Experiment, using KEK-PS and Super-Kamiokande”, 1995, unpublished; talk presented by M. Sakuda (K2K collaboration) at the *XXXth International Conference on High Energy Physics (ICHEP 2000)*, Osaka, Japan, July 2000.
- [6] MINOS Technical Design Report NuMI-L-337 October 1998.
- [7] See the OPERA web page at <http://www.cern.ch/opera/>
- [8] See the ICARUS/ICANOE web page at <http://pcnometh4.cern.ch/>
- [9] C. Athanassopoulos et al. (LSND Collab.), Phys. Rev. Lett. **77**, 3082 (1996); **81**, 1774 (1998); G. Mills, talk at *Neutrino-2000*, XIXth International Conference on Neutrino Physics and Astrophysics, Sudbury, Canada, June 2000.
- [10] A. Bazarko, MiniBooNE Collaboration, talk at *Neutrino-2000.*, S. Koutsoliotas et al., The MiniBooNE Technical Design Report.
- [11] These plots have been produced using the fast Monte Carlo simulation which is currently being used for the CNGS neutrino fluxes. The hadron production model is the BMPT parameterization which is thought to be the most complete parameterization of the existing data: M. Bonesini, A. Marchionni, F. Pietropaolo, T. Tabarelli de Fatis, hep-ph/0101163
- [12] NumI Facility Technical Design Report NuMI-346 March 1998.
- [13] V. Barger, S. Geer, R. Raja, K. Whisnant, hep-ph/0012017.
- [14] See the ORLaND web page <http://www.phys.subr.edu/orland/>
- [15] B. Richter, hep-ph/0008222.
- [16] Reference for GEANT and LEPTO here...
- [17] CNGS conceptual design report, CERN 98-02.
- [18] The ICARUS and NOE collaborations, ICANOE Proposal, chapters 4 and 5, CERN/SPSC 99-25 (1999).
- [19] D. Casper, private communication.
- [20] L. Wai, S. Wojcicki, B. Patterson, NuMI-L-713, hep-ph/0101090, and L. Wai, private communication.
- [21] H.M. Gallagher and M.C.Goodman, “Neutrino Cross Sections”, NuMI-112, 1995.
- [22] Second addendum to ICANOE proposal, CERN/SPSC 99-40 (Nov. 1999)
- [23] See P907 Proposal, <http://ppd.fnal.gov/experiments/e907/p907/p907.ps>

- [24] Proposal CERN/PS 214; see the HARP web page <http://harp.web.cern.ch/harp/>
- [25] See the NOMAD web page <http://nomadinfo.cern.ch/>
- [26] S. Mishra, private communication and NOMAD NIM paper in preparation.
- [27] C.K.Jung, (UNO Collab.)  
`\protect\vrule width0pt\protect\href{http://xxx.lanl.gov/abs/hep-ex/0005046}{hep-ex/0005046}`  
 and talk at the NNN00 workshop, August 2000.
- [28] F.Arneodo *et al.* (ICARUS and NOE Collab.), “ICANOE: Imaging and calorimetric neutrino oscillation experiment” CERN/SPSC 99-25, Addendum 1: Preliminary Technical Design & Cost Estimates, CERN/SPSC 99-39, both of which can be found at <http://pcnometh4.cern.ch>
- [29] Rough cost estimate, M.Goodman, private communication.
- [30] Rough cost estimate, Milind Diwan, private communication.
- [31] Super-Kamiokande Collaboration, Y. Fukuda et al., Phys. Lett. **B433**, 9 (1998); Phys. Lett. **B436**, 33 (1998); Phys. Rev. Lett. **81**, 1562 (1998); Phys. Rev. Lett. **82**, 2644 (1999).
- [32] M. Gell-Mann, R. Slansky, and P. Ramond, in *Supergravity* (North-Holland, 1979), p. 315; T. Yanagida, in *Proceedings of the Workshop on Unified Theory and Baryon Number in the Universe* (KEK, Japan, 1979).
- [33] V. Barger et al., Phys. Lett. **B437**, 107 (1998); A. Baltz, A. S. Goldhaber, and M. Goldhaber, Phys. Rev. Lett. **81**, 5730 (1998); R. Mohapatra and S. Nussinov, Phys. Rev. **D60**, 013002 (1999); G. Altarelli and F. Feruglio, Phys. Lett. **B439**, 112 (1998); C. Albright, K. Babu, and S. Barr, Phys. Rev. Lett. **81**, 1167 (1998); C. Albright and S. Barr, Phys. Lett. **B461**, 218 (1999).
- [34] KamLAND proposal, Stanford–HEP–98–03; A. Piepke, talk at *Neutrino–2000*, XIXth International Conference on Neutrino Physics and Astrophysics, Sudbury, Canada, June 2000.
- [35] M. Apollonio et al., Phys. Lett. **B420**, 397 (1998); Phys. Lett. **B466**, 415 (1999).
- [36] R. Bernstein and S. Parke, Phys. Rev. **D44**, 2069 (1991).
- [37] S. Petcov, Phys. Lett. **B434**, 321 (1998). M. Chiznov, M. Maris, S. Petcov, hep-ph/9810501; M. Chiznov, S. Petcov, hep-ph/9903424; M.Chiznov, S.Petcov, Phys. Rev. Lett. **83**,1096 (1999).
- [38] E. Akhmedov, A. Dighe, P. Lipari, A. Smirnov, Nucl. Phys. **B542**, 3 (1999); E. Akhmedov, Nucl.Phys. **B538**, 25 (1999); hep-ph/0001264.
- [39] V. Barger, S. Geer, K. Whisnant, Phys.Rev. **D61**, 053004 (2000).
- [40] V. Barger, S. Geer, R. Raja, K. Whisnant, Phys.Rev. **D62**, 013004 (2000); Phys.Rev. **D62**, 073002 (2000)
- [41] I. Mocioiu, R. Shrock, A.I.P. Conf. Proc. Conf. Proc. 533 (2000); I. Mocioiu, R. Shrock, Phys. Rev. **D62**, 053017 (2000).
- [42] J. Nelson, Private communication.
- [43] R. Stefanski, R. Bernstein, Private communication.

## 9 Appendix 1: Neutrino Masses and Mixing

In this appendix we briefly review the theoretical framework used to describe neutrino oscillations.

### 9.1 Neutrino mass

In the standard  $SU(3) \times SU(2)_L \times U(1)_Y$  model (SM) neutrinos occur in  $SU(2)_L$  doublets with  $Y = -1$ :

$$\mathcal{L}_{L\ell} = \begin{pmatrix} \nu_\ell \\ \ell \end{pmatrix}, \quad \ell = e, \mu, \tau \quad (6)$$

There are no electroweak-singlet neutrinos (often called right-handed neutrinos)  $\chi_{R,j}$ ,  $j = 1, \dots, n_s$ . Equivalently, these could be written as  $\overline{\chi}_{L,j}^c$ . There are three types of possible Lorentz-invariant bilinear operator products that can be formed from two Weyl fermions  $\psi_L$  and  $\chi_R$ :

- Dirac:  $m_D \overline{\psi}_L \chi_R + h.c.$  This connects opposite-chirality fields and conserves fermion number.
- Left-handed Majorana:  $m_L \psi_L^T C \psi_L + h.c.$  where  $C = i\gamma_2 \gamma_0$  is the charge conjugation matrix.
- Right-handed Majorana:  $M_R \chi_R^T C \chi_R + h.c.$

The Majorana mass terms connect fermion fields of the same chirality and violate fermion number (by two units). Using the anticommutativity of fermion fields and the property  $C^T = -C$ , it follows that a Majorana mass matrix appearing as

$$\psi_i^T C (M_{maj})_{ij} \psi_j \quad (7)$$

is symmetric in flavor indices:

$$M_{maj}^T = M_{maj} \quad (8)$$

Thus, in the SM, there is no Dirac neutrino mass term because (i) it is forbidden as a bare mass term by the gauge invariance, (ii) it cannot occur, as do the quark and charged lepton mass terms, via spontaneous symmetry breaking (SSB) of the electroweak (EW) symmetry starting from a Yukawa term because there are no EW-singlet neutrinos  $\chi_{R,j}$ . There is also no left-handed Majorana mass term because (i) it is forbidden as a bare mass term and (ii) it would require a  $I = 1, Y = 2$  Higgs field, but the SM has no such Higgs field. Finally, there is no right-handed Majorana mass term because there is no  $\chi_{R,j}$ . The same holds for the minimal supersymmetric standard model (MSSM) and the minimal  $SU(5)$  grand unified theory (GUT), both for the original and supersymmetric versions.

However, it is easy to add electroweak-singlet neutrinos  $\chi_R$  to the SM, MSSM, or  $SU(5)$  GUT; these are gauge-singlets under the SM gauge group and  $SU(5)$ , respectively. Denote these theories as the extended SM, etc. This gives rise to both Dirac and Majorana mass terms, the former via Yukawa terms and the latter as bare mass terms.

In the extended SM, MSSM, or  $SU(5)$  GUT, one could consider the addition of the  $\chi_R$  fields as *ad hoc*. However, a more complete grand unification is achieved with the (SUSY)  $SO(10)$  GUT, since all of the fermions of a given generation fit into a single

representation of  $\text{SO}(10)$ , namely, the 16-dimensional spinor representation  $\psi_L$ . In this theory the states  $\chi_R$  are not *ad hoc* additions, but are guaranteed to exist. In terms of  $\text{SU}(5)$  representations (recall,  $\text{SO}(10) \supset \text{SU}(5) \times \text{U}(1)$ )

$$16_L = 10_L + \bar{5}_L + 1_L \quad (9)$$

so for each generation, in addition to the usual 15 Weyl fermions comprising the  $10_L$  and  $5_R$ , (equivalently  $\bar{5}_L$ ) of  $\text{SU}(5)$ , there is also an  $\text{SU}(5)$ -singlet,  $\chi_L^c$  (equivalently,  $\chi_R$ ). So in  $\text{SO}(10)$  GUT, electroweak-singlet neutrinos are guaranteed to occur, with number equal to the number of SM generations, inferred to be  $n_s = 3$ . Furthermore, the generic scale for the coefficients in  $M_R$  is expected to be the GUT scale,  $M_{GUT} \sim 10^{16}$  GeV.

There is an important mechanism, which originally arose in the context of GUT's, but is more general, that naturally predicts light neutrinos. This is the seesaw mechanism [32]. The basic point is that because the Majorana mass term is an electroweak singlet, the associated Majorana mass matrix  $M_R$  should not be related to the electroweak mass scale  $v$ , and from a top-down point of view, it should be much larger than this scale. Denote this generically as  $m_R$ . This has the very important consequence that when we diagonalize the joint Dirac-Majorana mass matrix, the eigenvalues (masses) will be comprised of two different sets:  $n_s$  heavy masses, of order  $m_R$ , and 3 light masses. The largeness of  $m_R$  then naturally explains the smallness of the masses (or, most conservatively, upper bounds on masses) of the known neutrinos. This appealing mechanism also applies in the physical case of three generations and for  $n_s \geq 2$ .

At a phenomenological level, without further theoretical assumptions, there is a large range of values for the light  $m_\nu$ , since (1) the actual scale of  $m_R$  is theory-dependent, and (2) it is, *a priori*, not clear what to take for  $m_D$  since the known (Dirac) masses range over 5 orders of magnitude, from  $m_e, m_u \sim \text{MeV}$  to  $m_t = 174 \text{ GeV}$ , and this uncertainty gets squared. However, in the  $\text{SO}(10)$  GUT scheme, where one can plausibly use  $m_D \sim m_t$  for the third-generation neutrino, and  $m_R \sim M_{GUT} \sim 10^{16}$  GeV for the scale of masses in the right-handed Majorana mass matrix, one has

$$m(\nu_3) \sim \frac{m_t^2}{m_R} \sim 10^{-3} \text{ eV} \quad (10)$$

which is close to the value  $m(\nu_3) = 0.06 \text{ eV}$  obtained from  $\delta m_{atm}^2$  if one assumes a hierarchical neutrino mass spectrum with  $m(\nu_3) \gg m(\nu_2)$ . Thus, the seesaw mechanism not only provides an appealing qualitative explanation of why neutrino masses are much smaller than the masses of the other known fermions, but also, with plausible assumptions, predicts a value for  $m(\nu_3)$  comparable to suggestions from current atmospheric neutrino data.

## 9.2 Neutrino mixing and oscillations

The unitary transformation relating the mass eigenstates to the weak eigenstates is as follows,

$$\nu_{\ell_a} = \sum_{i=1}^3 U_{ai} \nu_i, \quad \ell_1 = e, \ell_2 = \mu, \ell_3 = \tau \quad (11)$$

i.e.,

$$\begin{pmatrix} \nu_e \\ \nu_\mu \\ \nu_\tau \end{pmatrix} = \begin{pmatrix} U_{e1} & U_{e2} & U_{e3} \\ U_{\mu1} & U_{\mu2} & U_{\mu3} \\ U_{\tau1} & U_{\tau2} & U_{\tau3} \end{pmatrix} \begin{pmatrix} \nu_1 \\ \nu_2 \\ \nu_3 \end{pmatrix} \quad (12)$$

One possible representation of this  $3 \times 3$  unitary matrix is

$$U = \begin{pmatrix} c_{12}c_{13} & s_{12}c_{13} & s_{13}e^{-i\delta} \\ -s_{12}c_{23} - c_{12}s_{23}s_{13}e^{i\delta} & c_{12}c_{23} - s_{12}s_{23}s_{13}e^{i\delta} & s_{23}c_{13} \\ s_{12}s_{23} - c_{12}c_{23}s_{13}e^{i\delta} & -c_{12}s_{23} - s_{12}c_{23}s_{13}e^{i\delta} & c_{23}c_{13} \end{pmatrix} \quad (13)$$

where  $c_{ij} = \cos \theta_{ij}$ ,  $s_{ij} = \sin \theta_{ij}$ . Thus, in this framework, the neutrino mixing depends on the four angles  $\theta_{12}$ ,  $\theta_{13}$ ,  $\theta_{23}$ , and  $\delta$ , and on two independent differences of squared masses,  $\delta m_{atm.}^2$ , which is  $\delta m_{32}^2 = m(\nu_3)^2 - m(\nu_2)^2$  in the favored fit, and  $\delta m_{sol.}^2$ , which may be taken to be  $\delta m_{21}^2 = m(\nu_2)^2 - m(\nu_1)^2$ . Note that these quantities involve both magnitude and sign; although in a two-species neutrino oscillation in vacuum the sign does not enter, in the three species oscillations relevant here, and including both matter effects and CP violation, the signs of the  $\delta m^2$  quantities do enter and can, in principle, be measured.

In the 1980's, most theorists thought that lepton mixing would be hierarchical, i.e. the lepton mixing matrix  $U$  would differ from the identity by small entries, and these would be smaller as one moved further from the diagonal, as is established to be the case with quark mixing. This was, indeed, a large part of the appeal of the MSW mechanism: it could produce large mixing with small vacuum mixing angles. However, the results from the SuperK measurements of atmospheric neutrinos have forced a revision in this conventional picture, providing strong evidence for essentially maximal mixing,  $\sin^2 2\theta_{23} = 1$ . A challenge to model-builders has thus been to get maximal  $\sin^2 2\theta_{23}$ . More recently, the SuperK solar neutrino data favors large  $\sin^2 2\theta_{12}$ . Bimaximal mixing schemes take  $\theta_{23} = \theta_{12} = \pi/4$  and  $\theta_{13} \ll 1$  [33]. There are no compelling theoretical suggestions concerning the magnitude of  $\theta_{13}$ , and one of the important physics goals for neutrino oscillation experiments with conventional beams is to try to measure this angle.

For our later discussion it will be useful to record the formulas for the various relevant neutrino oscillation transitions. In the absence of any matter effect, the probability that a (relativistic) weak neutrino eigenstate  $\nu_a$  becomes  $\nu_b$  after propagating a distance  $L$  is

$$\begin{aligned} P(\nu_a \rightarrow \nu_b) &= \delta_{ab} - 4 \sum_{i>j=1}^3 \text{Re}(K_{ab,ij}) \sin^2\left(\frac{\delta m_{ij}^2 L}{4E}\right) + \\ &+ 4 \sum_{i>j=1}^3 \text{Im}(K_{ab,ij}) \sin\left(\frac{\delta m_{ij}^2 L}{4E}\right) \cos\left(\frac{\delta m_{ij}^2 L}{4E}\right) \end{aligned} \quad (14)$$

where

$$K_{ab,ij} = U_{ai}U_{bi}^*U_{aj}^*U_{bj} \quad (15)$$

and

$$\delta m_{ij}^2 = m(\nu_i)^2 - m(\nu_j)^2 \quad (16)$$

Recall that in vacuum, CPT invariance implies  $P(\bar{\nu}_b \rightarrow \bar{\nu}_a) = P(\nu_a \rightarrow \nu_b)$  and hence, for  $b = a$ ,  $P(\bar{\nu}_a \rightarrow \bar{\nu}_a) = P(\nu_a \rightarrow \nu_a)$ . For the CP-transformed reaction  $\bar{\nu}_a \rightarrow \bar{\nu}_b$  and

the T-reversed reaction  $\nu_b \rightarrow \nu_a$ , the transition probabilities are given by the right-hand side of (14) with the sign of the imaginary term reversed. In the following we will assume CPT invariance, so that CP violation is equivalent to T violation.

The solar and atmospheric neutrino data indicate that

$$\delta m_{21}^2 = \delta m_{sol}^2 \ll \delta m_{31}^2 \approx \delta m_{32}^2 = \delta m_{atm}^2 \quad (17)$$

In this case, CP (T) violation effects are very small, so that in vacuum

$$P(\bar{\nu}_a \rightarrow \bar{\nu}_b) \simeq P(\nu_a \rightarrow \nu_b) \quad (18)$$

$$P(\nu_b \rightarrow \nu_a) \simeq P(\nu_a \rightarrow \nu_b) \quad (19)$$

In the absence of T violation, the second equality (19) would still hold in matter, but even in the absence of CP violation, the first equality (18) would not hold. With the hierarchy (17), the expressions for the specific oscillation transitions are

$$\begin{aligned} P(\nu_\mu \rightarrow \nu_\tau) &= 4|U_{33}|^2|U_{23}|^2 \sin^2\left(\frac{\delta m_{atm}^2 L}{4E}\right) \\ &= \sin^2 2\theta_{23} \cos^4 \theta_{13} \sin^2\left(\frac{\delta m_{atm}^2 L}{4E}\right) \end{aligned} \quad (20)$$

$$\begin{aligned} P(\nu_\mu \rightarrow \nu_e) &= 4|U_{13}|^2|U_{23}|^2 \sin^2\left(\frac{\delta m_{atm}^2 L}{4E}\right) \\ &= \sin^2 2\theta_{13} \sin^2 \theta_{23} \sin^2\left(\frac{\delta m_{atm}^2 L}{4E}\right) \end{aligned} \quad (21)$$

With units inserted, one has the general relation

$$\sin^2\left(\frac{\delta m^2 L}{4E}\right) = \sin^2\left(\frac{1.27(\delta m^2/\text{eV}^2)(L/\text{km})}{(E/\text{GeV})}\right) \quad (22)$$

This makes it clear what the approximate sensitivity of an experiment with a given pathlength is to a neutrino oscillation channel involving a given  $\delta m^2$ , for a beam with an energy  $E$ .

There can be significant corrections to the one- $\delta m^2$  oscillation formulas if  $\delta m_{sol}^2$  is at the upper end of the LMA range,  $\delta m_{sol}^2 \sim 10^{-4}$  eV<sup>2</sup>, if  $\sin^2 2\theta_{13}$  is sufficiently small. In this case, keeping dominant terms and neglecting possible small CP violating terms, eq. (21) becomes

$$\begin{aligned} P(\nu_\mu \rightarrow \nu_e) &= \sin^2 2\theta_{13} \sin^2 \theta_{23} \sin^2\left(\frac{\delta m_{atm}^2 L}{4E}\right) \\ &+ \sin^2 2\theta_{12} \cos^2 \theta_{13} \cos^2 \theta_{23} \sin^2\left(\frac{\delta m_{sol}^2 L}{4E}\right) \end{aligned} \quad (23)$$

Let us denote the two terms as  $T_1$  and  $T_2$ . As an illustrative example, let us consider a pathlength  $L$  sufficiently short that matter effects are not too important. Assume  $\sin^2 2\theta_{13} = 0.01$  and the upper end of the LMA solution, with  $\sin^2 2\theta_{12} = 0.8$  and  $\delta m_{sol}^2 = 10^{-4}$  eV<sup>2</sup>. Then for  $L = 730$  km,  $T_2 = 0.1T_1$ . For these values,  $\sin^2(\delta m_{atm}^2 L/(4E)) = 0.78$  while  $\sin^2(\delta m_{sol}^2 L/(4E)) = 0.95 \times 10^{-3}$ , so that the pathlength is causing a strong suppression of the subdominant oscillation due to  $\delta m_{sol}^2$ .

For sufficiently large  $L$  and small  $\sin^2 2\theta_{13}$ , the  $\delta m_{sol}^2$  oscillation can be a significant contribution to  $\nu_\mu \rightarrow \nu_e$ . However, we note that making  $L$  greater would mean that one would also have to make  $E$  greater to keep an acceptable event rate with a given detector, and this would tend to increase backgrounds to the  $\nu_\mu \rightarrow \nu_e$  signal. We also note that if KamLAND [34] achieves its projected sensitivity, it will have tested the LMA solution by  $\sim 2005$ .

In neutrino oscillation searches using reactor antineutrinos, i.e. tests of  $\bar{\nu}_e \rightarrow \bar{\nu}_e$ , the two-species mixing hypothesis used to fit the data is

$$P(\nu_e \rightarrow \nu_e) = 1 - \sin^2 2\theta_{reactor} \sin^2\left(\frac{\delta m_{reactor}^2 L}{4E}\right) \quad (24)$$

where  $\delta m_{reactor}^2$  is the squared mass difference relevant for  $\bar{\nu}_e \rightarrow \bar{\nu}_x$ . In particular, in the upper range of values of  $\delta m_{atm}^2$ , since the transitions  $\bar{\nu}_e \rightarrow \bar{\nu}_\mu$  and  $\bar{\nu}_e \rightarrow \bar{\nu}_\tau$  contribute to  $\bar{\nu}_e$  disappearance, one has

$$P(\nu_e \rightarrow \nu_e) = 1 - \sin^2 2\theta_{13} \sin^2\left(\frac{\delta m_{atm}^2 L}{4E}\right) \quad (25)$$

i.e.,  $\theta_{reactor} = \theta_{13}$ , and the Chooz reactor experiment yields the bound [35]

$$\sin^2 2\theta_{13} < 0.10 \quad (26)$$

which is also consistent with conclusions from the SuperK data analysis [31].

Further, the quantity “ $\sin^2 2\theta_{atm}$ ” often used to fit the data on atmospheric neutrinos with a simplified two-species mixing hypothesis, is, in the three-generation case,

$$\sin^2 2\theta_{atm} \equiv \sin^2 2\theta_{23} \cos^4 \theta_{13} \quad (27)$$

The SuperK data implies that (up to redefinitions of quadrants, etc.)

$$\theta_{23} \simeq \frac{\pi}{4} \quad (28)$$

and  $\sin^2 2\theta_{13} \ll 1$ . Thus, to good accuracy,  $\theta_{atm} = \theta_{23}$ .

The types of neutrino oscillations that can be searched for with a conventional neutrino beam include:

- $\nu_\mu \rightarrow \nu_\mu$  (disappearance)
- $\nu_\mu \rightarrow \nu_e, \nu_e \rightarrow e^-$  (appearance)
- $\nu_\mu \rightarrow \nu_\tau, \nu_\tau \rightarrow \tau^-; \tau^- \rightarrow (e^-, \mu^-) \dots$  (appearance)

Searches for the conjugate oscillation channels require  $\bar{\nu}_\mu$  beams. Since these have lower fluxes than  $\nu_\mu$  beams (and this difference can be large with sign-selected  $\pi$  beams that are decaying), one can concentrate on oscillation channels with  $\nu_\mu$  beams.

For neutrino oscillation experiments with pathlengths of order  $10^3$  km, matter effects are significant. These have been studied in a number of papers, e.g., [36, 37, 38, 39, 40, 41]. The constant density assumption provides a first approximation; realistic density profiles were included in the calculations of [39, 40, 41]. In the constant density approximation, for a simple two-species mixing, one has

$$P(\nu_a \rightarrow \nu_b) = \sin^2(2\theta_m) \sin^2(\omega L) \quad (29)$$

where

$$\sin^2(2\theta_m) = \frac{\sin^2(2\theta)}{\sin^2(2\theta) + \left[ \cos(2\theta) - \frac{2\sqrt{2}G_F N_e E}{\delta m^2} \right]^2} \quad (30)$$

$$\omega^2 = \left[ \frac{\delta m^2}{4E} \cos(2\theta) - \frac{G_f}{\sqrt{2}} N_e \right]^2 + \left[ \frac{\delta m^2}{4E} \sin(2\theta) \right]^2 \quad (31)$$

where  $N_e$  is the electron number density of the matter.

## 10 Appendix 2: Detector unit costs

Estimating the unit costs for each detector type is not straightforward. We can base our cost estimates on detectors that are currently under construction, or have recently been proposed. However, these example detectors have been proposed/costed at different times using different accounting systems in different currencies with different levels of external scrutiny. To attempt to compare like-with-like we have started from the bare materials and services (M&S) costs of the detector itself, which we have corrected to include salaries (SWF), engineering and R&D (EDIA) costs. The scaling factors were determined for a current US-based neutrino detector (MINOS). An estimate of overheads and contingencies (35%) has been included to reflect the “fully-loaded” costs associated with a US-based detector. Finally, the resulting unit costs have been corrected for inflation to correspond to FY01 dollars. Based on the fully loaded FY01 unit costs, for each detector type the mass of the detectors that could be built with a budget of \$500M can be estimated. The costs for a cavern for each detector technology is based on the recent UNO estimates for a hard rock cavern (\$200/m<sup>3</sup>) using the computed detector masses and the densities of the various detector media [27]. The results are summarized in Table 5.

The bare detector costs are based on the following:

- (i) The water cherenkov detector estimates are based on those documented in the UNO cost estimate [27], and correspond to 237M\$/450 kt (FY00 dollars), assuming 10% photomultiplier coverage in the entire detector. We assume a hard rock site rather than the proposed WIPP site. The actual UNO proposal is based on 40% photomultiplier coverage in the central third of the detector’s volume, which is optimized for certain proton decay and astrophysical neutrino channels. These physics topics are the driving force behind the UNO proposal.
- (ii) The liquid argon unit cost is based on the Icaroe costs of 14.4 MEuro per 1.9 kt module, with \$0.9425 per/Euro (FY99 dollars). Note the costing presented in this document assumes only cryogenic modules [28].
- (iii) The steel-scintillator unit cost is based on the MINOS M&S unit cost, which is based on the most recent (2/01) far-detector cost data giving a total of 16.3M\$ (FY98 dollars) [6, 42]. The total far detector (5.4 kt) cost including R&D, labor, and institutional overhead costs in then-year dollars is 25.4M\$.
- (iv) The mineral oil cerenkov unit cost is based on the MiniBooNE M&S unit cost, which is based on TDR detector costs (FY00 dollars) [10, 43].

Table 5: Detector cost estimates.

	Water Cerenkov	Mineral Oil Cerenkov	Liquid Argon	Steel/ Scintillator
Bare Unloaded Unit Cost (M\$/kt)	0.36	1.3	7.1	3.0
Unloaded Unit Cost (M\$/kt) <sup>a)</sup>	0.57	1.75	11.2	4.7
FY for estimates	2000	2000	1999	1998
Loaded Unit Cost (M\$/kt) <sup>b)</sup>	0.67	1.92	13.5	5.9
Mass (kt) per \$500M	745	261	37	85
Medium density (g/cm <sup>3</sup> )	1.0	0.9	1.8	3.5
Cavern cost (M\$) <sup>c)</sup>	106	41	2.9	3.4

a) M&S + SWF + EDIA

b) FY01 costs including overhead and 35% contingency

c) Note that deep caverns are not necessarily needed.